

Accepted for publication in the Astrophysical Journal

## Biases on initial mass function determinations. II. Real multiple systems and chance superpositions<sup>1</sup>

J. Maíz Apellániz<sup>2,3</sup>

*Instituto de Astrofísica de Andalucía-CSIC, Camino bajo de Huétor 50, 18008 Granada, Spain*

### ABSTRACT

When calculating stellar initial mass functions (IMFs) for young clusters, one has to take into account that most massive stars are born in multiple systems and that most IMFs are derived from data that cannot resolve such systems. It is also common to measure IMFs for clusters that are located at distances where multiple chance superpositions between members are expected to happen. In this article I model the consequences of both of those phenomena, real multiple systems and chance superpositions, on the observed color-magnitude diagrams and the IMFs derived from them. Using numerical experiments I quantify their influence on the IMF slope for massive stars and on the generation of systems with apparent masses above the stellar upper mass limit. The results in this paper can be used to correct for the biases induced by real and chance-alignment multiple systems when the effects are small and to identify when they are so large that most information about the IMF in the observed color-magnitude diagram is lost. Real multiple systems affect the observed or apparent massive-star MF slope little but can create a significant population of apparently ultramassive stars. Chance superpositions produce only small biases when the number of superimposed stars is low but, once a certain number threshold is reached, they can affect both the observed slope and the apparent stellar upper mass limit.

---

<sup>1</sup>This article is partially based on observations made with the NASA/ESA Hubble Space Telescope (HST), some of them associated with GO program 10602 and the rest gathered from the archive, obtained at the Space Telescope Science Institute, which is operated by the Association of Universities for Research in Astronomy, Inc., under NASA contract NAS 5-26555.

<sup>2</sup>e-mail contact: jmaiz@iaa.es.

<sup>3</sup>Ramón y Cajal fellow.

In the second part of the paper, I apply the experiments to two well known massive young clusters in the Local Group, NGC 3603 and R136. In both cases I show that the observed population of stars with masses above  $120 M_{\odot}$  can be explained by the effects of unresolved objects, mostly real multiple systems for NGC 3603 and a combination of real and chance-alignment multiple systems for R136. Therefore, the case for the reality of a stellar upper mass limit at solar or near-solar metallicities is strengthened, with a possible value even lower than  $150 M_{\odot}$ . An IMF slope somewhat flatter than Salpeter or Kroupa with  $\gamma$  between  $-1.6$  and  $-2.0$  is derived for the central region of NGC 3603, with a significant contribution to the uncertainty arising from the imprecise knowledge of the distance to the cluster. The IMF at the very center of R136 cannot be measured with the currently available data but the situation could change with new Hubble Space Telescope (HST) observations.

*Subject headings:* binaries: general — binaries: visual — methods: numerical — methods: statistical — stars: luminosity function, mass function — open clusters and associations: individual (NGC 3603, 30 Doradus)

## 1. Introduction

This paper is the second one of a series where we explore the effects of different biases on the determination of the stellar initial mass function (IMF). In paper I (Maíz Apellániz & Úbeda 2005) we analyzed the numerical biases induced by using bins of equal width when fitting power-laws to binned data (an effect that is more general than its application to the calculation of mass functions). Those biases can be eliminated in several ways, of which a simple one is by grouping the data in equal-number bins (as opposed to equal-width bins). In this second paper I explore the effect of unresolved multiple systems, either physical or chance alignments, especially for the high-mass end of the IMF. In a future paper we will analyze the effect of random uncertainties in the mass determinations on the computed initial mass function<sup>1</sup>.

---

<sup>1</sup>Most of the analysis in these papers is also applicable to the calculation of the present-day mass function (PDMF).

### 1.1. Binaries and the IMF

Why worry about binaries and higher-order multiple systems when calculating the IMF of a young stellar cluster such as NGC 3603 or R136? The quick answer is because one expects most of the observed point sources in clusters beyond a few kpc to be multiple. Therefore, deriving their masses by assuming they are single stars should introduce biases in the determination of the stellar mass functions of the clusters.

Mason et al. (1998) studied nearby O stars from a sample that included field objects and stars in low- and intermediate-mass clusters and associations. They analyzed the observed multiple fractions as a function of environment, including both spectroscopic and visual/speckle binaries and discovered that at least 72% of the O stars in clusters and associations had detected companions. Furthermore, the period distribution had a clear bimodal structure, with one peak around 10 days and another one around  $10^5$  years. They argued that such an effect was quite likely to be instrumental because binaries with periods  $P$  near 1-1000 years are hard to detect and because the period distribution for B stars is quite flat<sup>2</sup>. Therefore, Mason et al. (1998) predicted that when better spatial resolution were achieved and more intensive radial-velocity variation surveys were undertaken in the future, the gap between the two peaks might be filled and the true multiple fraction for massive stars in clusters might be found to be close to unity. Another interesting result of that paper was that the mass-ratio distribution for O binaries was flat or nearly so, i.e. massive stars tend to have companions that are more massive on average than what would be expected from a random sampling of the IMF. The shape of the secondary mass distribution function is relevant because different slopes should affect the observed or apparent mass function derived from unresolved data in different ways. Sagar & Richtler (1991) calculated that the apparent MF slope for intermediate-mass stars in the random pairing case becomes significantly flatter when adding unresolved binaries but the effect is likely to be different in the flat mass-ratio case.

In the ten years after Mason et al. (1998) other works have validated their conclusions. García & Mermilliod (2001) measured that 11 out of 14 O-systems in the cluster NGC 6231 are spectroscopic binaries. This means that at least 79% of its O/WR systems are multiple and at least 88% of their O/WR (and some early B) stars are in multiple systems. Their numbers are also similar for early-B stars. Also, new studies are indeed filling the Mason period gap: Gamen et al. (2007) reported 11 new massive spectroscopic binaries and Maíz Apellániz et al. (2008b) cite two new visual systems in the solar neighborhood

---

<sup>2</sup>Such a distribution, expressed in terms of separation  $r$  instead of  $P$ , is close to  $f(\log r) \propto (\log r)^0$  and is known as Öpik’s law, after Öpik (1924).

(see also Nelan et al. 2004). With respect to the secondary mass distribution function, Kouwenhoven et al. (2005) studied intermediate-mass stars in the Sco OB2 association and found that they could exclude random pairing in binaries, since the more massive stars clearly tend to associate with other massive objects. Another recent study of Cyg OB2 by Kobulnicky & Fryer (2007) also finds a large ( $>80\%$ ) binary fraction for massive stars. Those authors favor a secondary mass distribution function that is either (a) nearly flat or (b) a combination of a 60% Kroupa-like distribution and a 40% “twin” ( $M_2 > 0.95M_1$ ) component.

But what about more massive clusters? Is it possible that the multiple fraction there is significantly lower? Studying distant objects is more complicated but a recent survey by Evans et al. (2006) found that NGC 346 (in the SMC), NGC 2004, and N11 (in the LMC) have a minimum spectroscopic binary fraction for O- and early B-type stars of 23 to 36%. Considering that their program did not allow them to detect binaries with periods of more than several tens of days and that at the distance of the Magellanic Clouds it is very hard to resolve visual binaries, the real binary fraction should be considerably higher. Therefore, it is safe to conclude that the effect of unresolved massive binaries in the observed IMF is important and needs to be analyzed. Such an analysis is the first goal of this paper.

## 1.2. The stellar upper mass limit

From the point of view of the origin of the IMF, it has become apparent in the last decade that massive stars must form in a different way than low-mass objects because of the short time scales involved and the limiting effect of radiation pressure on the mass accretion rate (Bally & Zinnecker 2005; Zinnecker & Yorke 2007). There are currently two viable alternatives to form a massive star: by accretion through a disk, either in a relatively isolated environment or in a more crowded one where competition for mass among different protostars may be important, and by stellar collisions followed by mergers. The second alternative can only be relevant when the stellar densities are very high, such as at the core of a dense and massive cluster, but cannot be significant in relatively low-density environments such as OB associations.

If stellar mergers are indeed important at the core of dense clusters, there should be large consequences on their stellar IMFs. Portegies Zwart et al. (1999) predicted that runaway collisions in such cores will lead to stars with masses above  $100 M_\odot$  in a time scale of one or a few million years, which is comparable to the expected life times of those stars. The process may keep going on to the point of producing objects above  $1000 M_\odot$  that would end up as intermediate-mass black holes (Portegies Zwart et al. 2004). Therefore, massive

dense clusters should show an stellar upper mass limit  $m_{\text{max}}$  significantly higher than those of lower density or mass. Can such stellar behemoths exist? Recently, Belkus et al. (2007) and Yungelson et al. (2008) have attempted modeling of solar-metallicity stars up to  $1000 M_{\odot}$ , which would be formed by mergers. However, such modeling encounters problems with the determination of the Eddington limit, its associated instabilities and interaction with rotation, and with the large extrapolation required for mass-loss rates (which are already uncertain at the present time even for run-of-the-mill main-sequence O stars). Hence, theory has not given its final word on the possible existence of such ultramassive stars.

What do observations tell us about those hypothetical ultramassive stars? Several papers on R136 and other Local Group massive young clusters (Weidner & Kroupa 2004; Figer 2005; Oey & Clarke 2005; Koen 2006) indicate that  $m_{\text{max}} \approx 120\text{-}200 M_{\odot}$  when evolutionary tracks are used to obtain stellar masses<sup>3</sup>. Some luminous blue variables (LBVs) such as  $\eta$  Car could have slightly higher evolutionary masses but LBVs are notoriously difficult to observe in detail due to the existence of circumstellar material. With respect to the more accurate masses measured from the orbital motion of the stars (keplerian masses), the highest published values correspond to WR 20a, a binary with  $83.0 \pm 5.0 M_{\odot}$  and  $82.0 \pm 5.0 M_{\odot}$  (Bonanos et al. 2004, see also Rauw et al. 2004). Therefore, on a first impression it appears that observations do not favor the existence of ultramassive stars at near-solar metallicity.

Unresolved multiple systems can also play a role in the identification of ultramassive stars by making e.g. a binary made out of two stars close to the stellar upper mass limit appear as a single object with an evolutionary mass well above that limit. For example, Maíz Apellániz et al. (2007) found that Pismis 24-1, formerly an ultramassive star candidate, is in reality composed of three stars with masses below  $120 M_{\odot}$ . It is also possible that the observed  $m_{\text{max}}$  measured from evolutionary masses is affected not only by real (bound) multiple systems but also by chance alignments in the crowded environments where some of these objects are found. Analyzing the possibility that some of the objects observed close to  $m_{\text{max}}$  may be blended sources composed of stars of significantly lower mass is the second goal of this paper.

## 2. Experiments

In order to test the effect of unresolved binaries and blending on the massive-star IMF slope and the stellar upper mass limit I have designed three numerical experiments. The first one analyzes the effect of real binaries, the second one that of chance superpositions,

---

<sup>3</sup>Those values are called evolutionary masses and refer to the initial mass of the star.

and the third one combines the two effects. The purpose of the experiments is to analyze the effects on a simple test IMF, provide a way to correct them, and describe the tools needed to extend the technique to other circumstances.

I design the simple case by assuming a well-sampled single stellar population with an age of 1 million years and solar metallicity. The choices for the age and metallicity are given by our desire to test our results with an analysis of NGC 3603 and R136 (note that the latter is currently thought to be of somewhat lower metallicity and may be slightly older) and by the simplicity of not having objects clearly evolved off the main sequence or even collapsed. Since we are only interested in the behavior of the top part of the IMF, for simplicity I assume that all the stars have already reached the main sequence, even though such an assumption should not valid for the low-mass stars. The  $T_{\text{eff}}$ ,  $\log g$ , and  $\log L$  information was obtained from the Geneva evolutionary tracks and isochrones database by Lejeune & Schaerer (2001) selecting the case with standard mass-loss rates and no rotation<sup>4</sup>. For masses below  $0.8 M_{\odot}$  I use the  $M_V$  calibration of Kroupa et al. (1993) to extend the isochrone until  $0.1 M_{\odot}$ . For the value of  $m_{\text{max}}$ , I select the highest value available in the Geneva tracks,  $120 M_{\odot}$ , which is on the low end of the possible range (for  $m_{\text{max}}$ ) for solar and near-solar metallicities. The 1-million-year isochrone was inserted into the new evolutionary synthesis module of CHORIZOS (Maíz Apellániz 2004) to calculate the Johnson  $U$  and  $V$  absolute magnitudes<sup>5</sup> as a function of mass using different synthetic spectral energy distributions (SEDs) as a function of  $T_{\text{eff}}$ : TLUSTY (Lanz & Hubeny 2003, 2007), Kurucz (Castelli & Kurucz 2003), and Lejeune (Lejeune et al. 1998) for the high, intermediate, and low temperature ranges, respectively. The Johnson zero points derived by Maíz Apellániz (2006) and modified by Maíz Apellániz (2007) were used. The final results are two tabulated, finely-gridded functions that give  $V$  and  $U - V$  as a function of mass  $m$  between  $0.1$  and  $120 M_{\odot}$ . The two functions were then extrapolated in  $\log m$  up to  $m = 1000 M_{\odot}$  ( $\log m = 3$ ). Note that  $V(m)$  is a strict monotonically decreasing function over the full range of  $m = 0.1 - 1000 M_{\odot}$  (this is true for the chosen isochrone but it is not true in general). Therefore, it is possible to invert it to produce  $m(V)$ , which gives the true mass<sup>6</sup> that corresponds to a star of absolute magnitude  $V$ .

---

<sup>4</sup>In the last years much work has been done on new evolutionary tracks and isochrones with rotation and possibly-reduced mass-loss rates due to clumping corrections. The present work can be easily adapted to those other conditions but the effects on our results are expected to be relatively minor.

<sup>5</sup>For the sake of notation simplicity and since at this point I am not discussing distance effects, I write  $M_U$  and  $M_V$  simply as  $U$  and  $V$ , respectively.

<sup>6</sup>Throughout this paper  $m$  is considered to be the initial stellar mass, not the mass when the star is 1 million years old.

Once  $V(m)$  and  $U(m) - V(m)$  as a function of mass have been generated, I calculate the corresponding bidimensional single-star color-magnitude density function  $g_{1s}(U - V, V)$  by applying one of two cases: [a] a Kroupa IMF, which can be described as a continuous function comprised of two power law segments  $dn/dm = f(m) \propto m^\gamma$ , with  $\gamma = -1.3$  for  $m = 0.1 - 0.5 M_\odot$  and  $\gamma = -2.3$  for  $m = 0.5 - 120 M_\odot$ ; [b] a flatter, top-heavy IMF, similar to Kroupa but with  $\gamma = -1.3$  for  $m = 0.1 - 0.5 M_\odot$  and  $\gamma = -2.0$  for  $m = 0.5 - 120 M_\odot$ .  $g_{1s}(U - V, V)$  can be collapsed into a one-dimensional magnitude function<sup>7</sup>  $G_{1s}(V)$  without losing any information because for our isochrone  $V(m)$  is a strictly monotonic function. Since both  $g_{1s}(U - V, V)$  and  $G_{1s}(V)$  are functions defined in a fine (2-D and 1-D, respectively) grid, special care has to be taken to avoid introducing numerical biases and noise due to sampling and interpolation.

Finally, in order to reproduce the blending problems associated with the strategy commonly used to derive evolutionary masses from luminosity functions, I combine individual stars into blended objects according to different rules. This is done by adding their  $U$ - and  $V$ -band luminosities and computing the resulting  $V$  and  $U - V$  values. From there, I generate: [a] a new bidimensional color-magnitude density function  $g_x(U - V, V)$  from  $g_{1s}(U - V, V)$ , where  $x$  specifies the combination rule, and [b] the apparent mass function  $f_{a,x}(m_a)$  calculated by collapsing  $g_x(U - V, V)$  into  $G_x(V)$  and then converting the observed absolute magnitudes into apparent masses. The last step is done by applying  $m(V)$ , which is a relationship derived for individual stars that is not correct for blended objects. Therefore, the derived apparent masses  $m_a$  are not the real ones. In other words, I am deriving an apparent mass function (AMF) by [a] assuming that all the observed objects are single stars (even though they are not) and [b] using only the absolute magnitudes (but not their colors) to obtain the masses. The first assumption is applied in most IMF studies. The second assumption should be valid as long as all the stars are at the same distance, extinction is well known, contamination by field objects or stars of different ages is negligible, and  $m(V)$  is a strictly monotonic function. Note, however, that for ages older than  $\approx 2.5$  million years (when  $m(V)$  is no longer monotonic) the same type of analysis can still be done measuring masses by minimizing the distance to a given isochrone.

Note also that I am not using spectral types for the calculation of the IMF. For massive stars, the main advantages of using spectral types to calculate IMFs are a better determination of the cluster age, a direct knowledge of the intrinsic color of the star (hence, usually a better extinction measurement), and an ability to derive additional luminosity/distance information. Those are all possible sources of biases, so spectroscopy indeed represents an

---

<sup>7</sup>In this paper I use magnitude functions instead of luminosity functions; the conversion between one and the other is straightforward.

improvement over a pure photometric analysis. However, as previously stated, for the experiments in this paper I assume that age, extinction, and distance are all well constrained by external information, so those advantages of spectroscopy are not relevant for our discussion. The additional advantage that spectroscopy has over a simple color-magnitude analysis when blended sources are present is the possibility of identifying them by their composite spectra (something that can also be done in some cases with multi-filter photometry). Note, however, that many spectra of blended sources cannot be distinguished from those of single ones for three possible reasons: [a] need of very high S/N data to detect the contribution from a dim companion, [b] absence of time-resolved data to detect spectroscopic binaries, and [c] similarity between the two blended spectra<sup>8</sup>. In summary, spectroscopy can be and in most cases is a helpful aid to the elimination of biases in IMF determinations but it also has its costs and limitations in detecting blended sources. This paper should not be interpreted as neglecting the importance of spectroscopy for the study of the massive-star IMF but rather as a study of what can be done when spectroscopy is not available.

## 2.1. Experiment 1: Real binaries

For the first experiment I attempt to reproduce the effect of unresolved multiple systems which, for simplicity, I assume to be always binaries. The combination rules applied in this case are:

1. Each star is blended with one and only one star.
2. For a blended system with  $m_1 \geq m_2$ ,  $m_2$  is randomly selected from a flat distribution in mass between  $0.1 M_\odot$  (the lower mass limit) and  $m_1$ . The pairing is done while keeping the real, single-mass stellar IMF as Kroupa (case a) or top-heavy (case b).

This experiment reproduces the physical situation in which all the stars in a cluster are binaries with a flat mass-ratio distribution. As previously discussed, this is a rather accurate approximation for systems with at least one massive star but is likely to be more imprecise for lower-mass objects. For example, Reipurth et al. (2007) observe only an 8.8% binary fraction among low-mass stars in the Orion Nebula Cluster and Sollima et al. (2007) detect a binary fraction of  $\approx 40\%$  for globular clusters with ages less than  $10^{10}$  years (of course, the

---

<sup>8</sup>For example, the spectra of the two components of WR 20a (Bonanos et al. 2004) are almost indistinguishable and if it were not for the large velocity variations induced by their proximity it would be almost impossible to identify the spectrum as a composite.



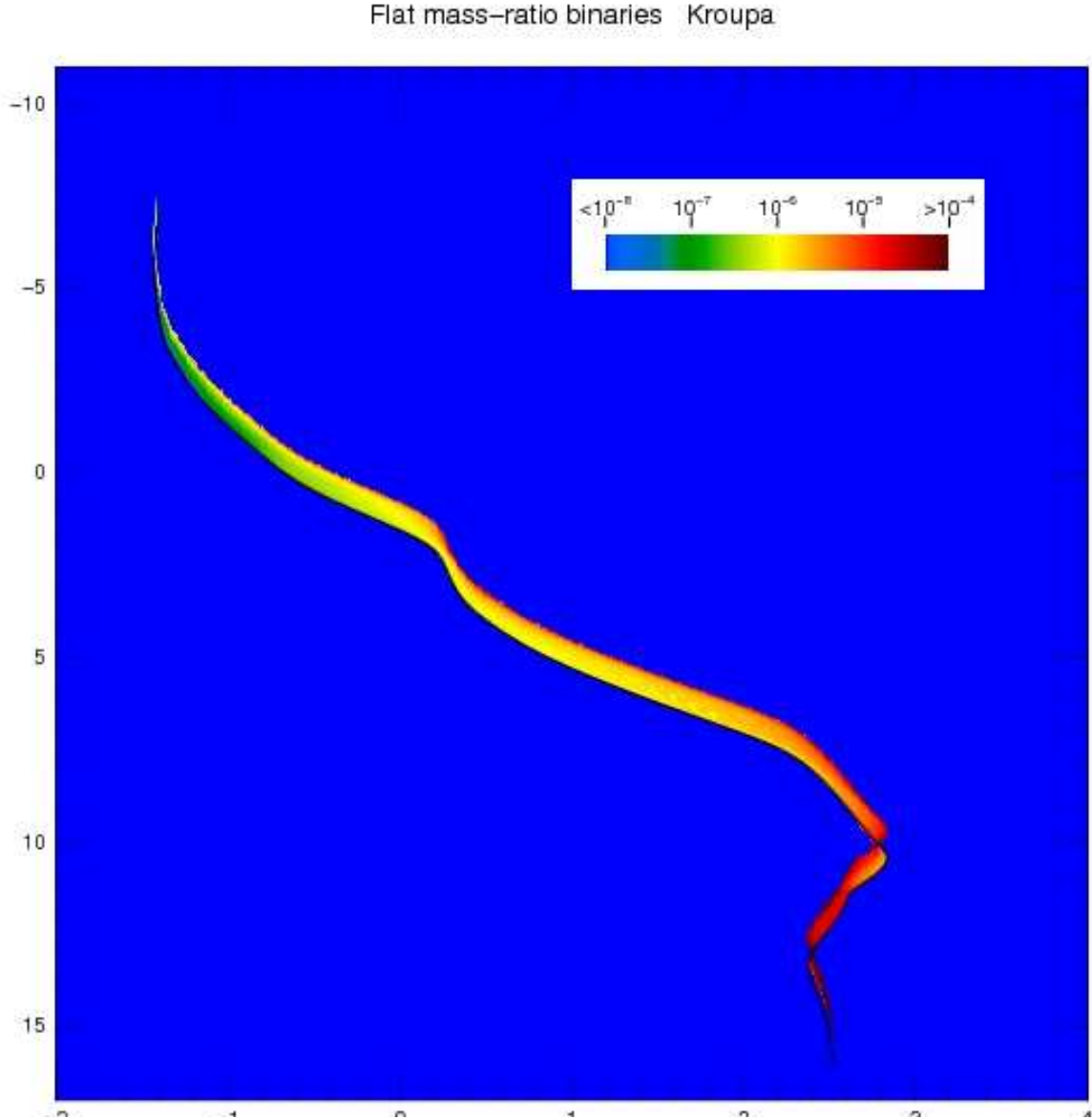


Fig. 1.— Color-magnitude density function  $g_{1b}(U - V, V)$  for the Kroupa case of experiment 1 (real binaries) shown as a Hess diagram. The black line shows the position of the 1 million year isochrone. The function scaling is logarithmic and the normalization is arbitrary. See the electronic version of the journal for a color version of this figure.

situation in globular clusters is complicated by dynamical evolution, as the lower fraction detected by the same authors for older clusters show). However, since our goal is to study the top part of the resulting AMF, the validity of the approximation for low-mass objects should not concern us much. The other assumption in this experiment is that all massive binaries are unresolved. Under what circumstances is that reasonable? As previously described, in the solar neighborhood ( $\lesssim 2$  kpc)  $\sim 1/3$  of the massive systems in clusters/associations are spectroscopic binaries, another  $\sim 1/3$  are visual/interferometric multiple systems, and the remaining  $\sim 1/3$  could be undetected multiples (with periods approximately between those of the detected spectroscopic and visual/interferometric systems)<sup>9</sup>. This means that even in the solar neighborhood  $\sim 2/3$  of the massive binary systems would appear as point sources in a ground-based imaging study with standard imaging techniques. Using better spatial resolution (e.g. HST or non-standard techniques such as adaptive optics or lucky imaging) buys you a larger fraction of resolved systems in the solar neighborhood but once you reach several kpc, even that is not enough. For example, ACS/HRC (the imager with the best spatial resolution on HST) can still resolve objects with a magnitude difference  $\Delta m \approx 1$  mag and a separation of 50 mas but that is close to the limit of its capabilities (see e.g. Maíz Apellániz et al. 2008b). At a distance of 7 kpc, 50 mas corresponds to 350 AU, which is the typical value for the separation in the visual O-systems of Mason et al. (1998), implying that at that distance ACS/HRC would resolve only 20-30% of the massive binary systems (if their properties are similar to those in the solar neighborhood). The LMC is hopeless, even with HST: 50 mas corresponds to 2500 AU, so only very-large separation systems are resolved. Therefore, I can conclude that this experiment represents a reasonable approximation to the conditions in many IMF studies of young clusters and associations beyond the solar neighborhood.

The resulting color-magnitude density function,  $g_{1b}(U - V, V)$  is shown in Fig. 1 for the Kroupa IMF case (the top-heavy equivalent function is not shown but is visually very similar).  $g_{1b}(U - V, V)$  is zero nearly everywhere in the color-magnitude diagram except in the narrow band between the original isochrone and a near-parallel line that is located approximately 0.75 magnitudes above it (the location of the equal-mass binaries). The band between the two lines is filled with the non-equal-mass binaries. At the low-mass extreme the band becomes narrower and detached from the isochrone because the addition of any companion changes the magnitude (and possibly the color) considerably. That effect does not take place for higher masses because the addition of a  $0.1 M_{\odot}$  star is undetectable in color-magnitude with the scale of Fig. 1. At the high-mass end an obvious extension beyond

---

<sup>9</sup>It should be pointed out that the overlap between spectroscopic and visual/interferometric systems is very small, see Boyajian et al. (2007) and North et al. (2007) for examples.

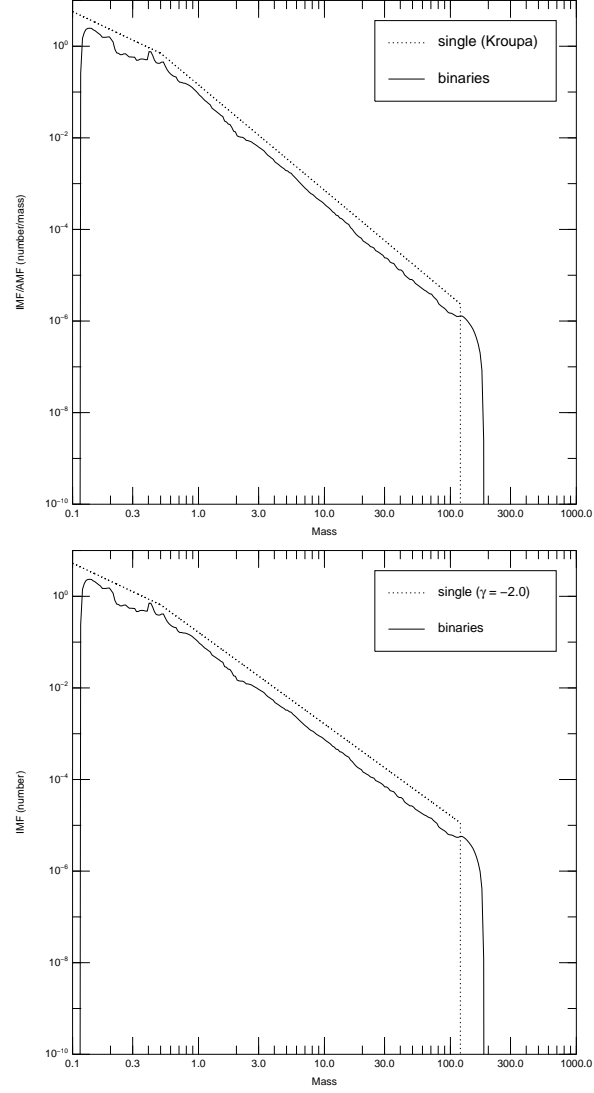


Fig. 2.— (Real) IMF and AMF for experiment 1 (real binaries). The top panel shows the Kroupa case and the bottom panel the top-heavy case. The mass is expressed in solar units. The IMF is normalized to 1.0 and the AMF to 0.5.

$m_{\max}$  is observed. The extension is nearly vertical because massive stars of this age have near-degenerate  $U - V$  colors. The apparent upper mass limit,  $m_{\max,1b}$  is well defined and has a value of  $182 M_{\odot}$ .

The calculated AMFs for the Kroupa and top-heavy cases are shown in Fig. 2 along with the original IMFs. The behavior in both cases is similar. For low masses, the apparent lower limit is slightly shifted towards higher values (corresponding to a  $0.1 M_{\odot} + 0.1 M_{\odot}$  binary, since  $0.1 M_{\odot}$  is the lower mass limit of our experiments) and several peaks in the AMF can be seen below  $0.7 M_{\odot}$  due to the fine structure of  $m(V)$ <sup>10</sup>. For intermediate and high masses, the AMF runs nearly parallel to the IMF at a value roughly 1/2 of the IMF (the AMF includes one half of the systems of the IMF). In order to quantify the change in slope between the IMF and the binary AMF,  $\Delta\gamma$ , I have fitted a power law to a number of mass ranges using the technique in Paper I. Results are plotted in Fig. 3. For  $m_{\text{lower}}$  between 1 and  $16 M_{\odot}$  and  $m_{\text{upper}} \neq 120 M_{\odot}$  there is a steepening of the MF with  $\Delta\gamma$  between  $-0.2$  and  $0.0$  while for larger masses in most cases there a slight flattening with  $\Delta\gamma$  between  $0.0$  and  $0.2$ .  $\Delta\gamma$  depends only weakly on  $m_{\text{upper}}$  and the IMF slope. Note that some of the small-scale structure observed in Fig. 3 at the 0.02 level may be of numerical origin. I conclude that for most cases *the existence of unresolved binaries has only a small effect on the massive-star IMF slope*.

The largest difference between the IMF and the AMF happens beyond  $m_{\max}$ , where a tail is formed in the AMF: these are the apparently ultramassive stars (AUMSs). In Table 1 I quantify the effect by giving the apparent number ratios between the objects above  $m_{\max}$  and the objects in different ranges below it. There is a strong dependence on the IMF slope, since a top-heavy IMF allows a significantly larger number of objects to become AUMSs.

Figure 1 reveals another interesting issue which is relevant to IMF studies of Galactic clusters, where distance is one of the unknowns that has to be solved for. O stars are notoriously difficult to use as yardsticks because their near-degenerate optical colors place them along near-vertical lines in a color-magnitude diagram (see e.g. Fig. 1 but see also Maíz Apellániz & Sota 2008 for recent progress on improving our knowledge of O-stars colors). For that reason, main-sequence B stars (which have intrinsic  $U - V$  in the approximate range from  $-1.3$  to  $-0.1$ ) are more commonly used to derive distances with main-sequence fitting techniques. However, if the assumption which underlies our experiment is relevant (that most O and B stars are unresolved binaries with flat mass-ratio distributions), then it is

---

<sup>10</sup>The conversion from a magnitude or luminosity function to a IMF involves  $dm/dV$ , whose numerical behavior may be odd when using coarsely-gridded tabular information to derive it. The observed structures may or may not be real but since our concern is with the high-mass end of the AMF, we will not discuss them any further.

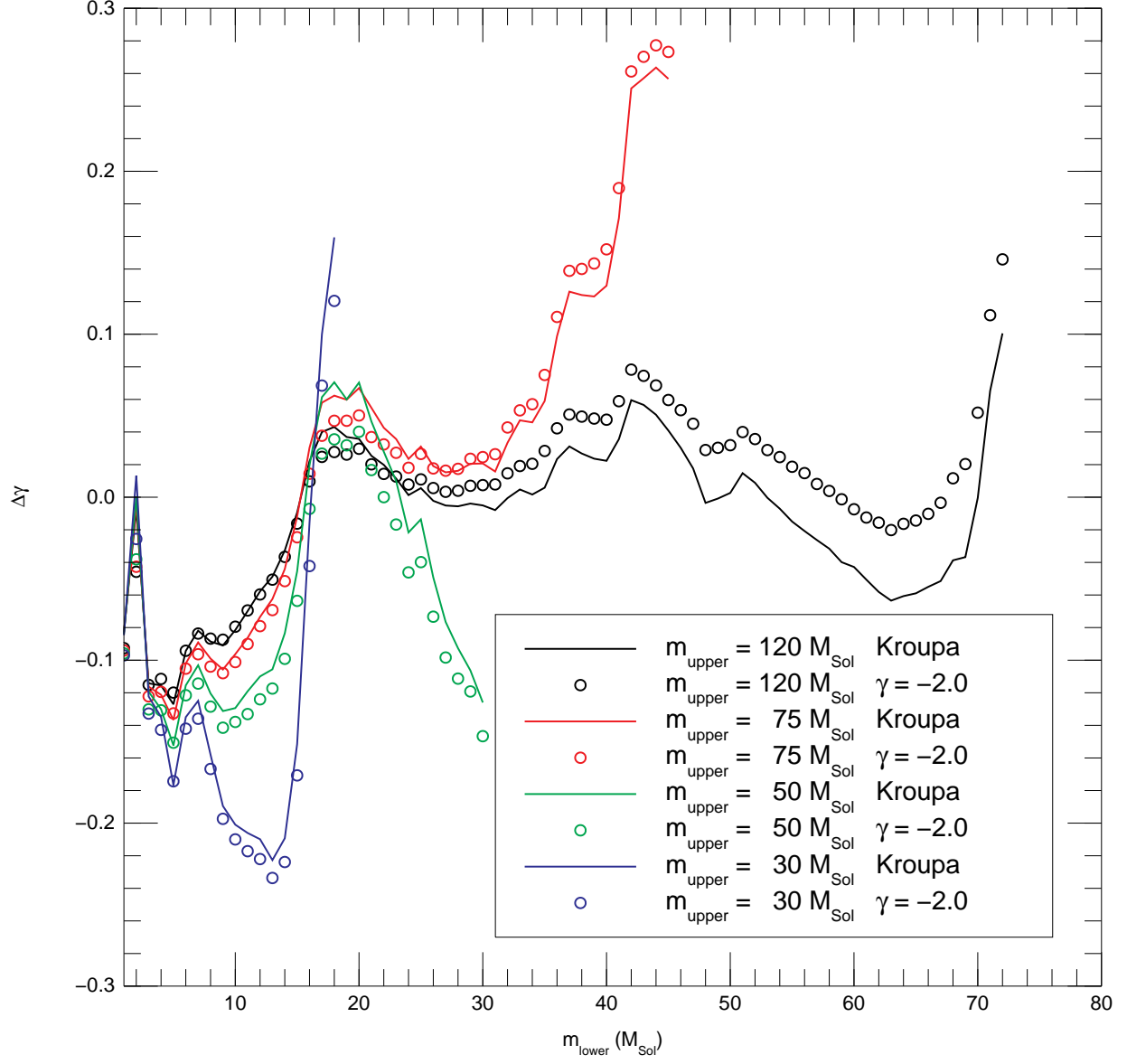


Fig. 3.— Slope change introduced by flat mass-ratio binaries (first experiment) as a function of the lower limit for the mass range ( $m_{\text{lower}}$ ) for the two IMF cases and for different values of the upper limit for the mass range ( $m_{\text{upper}}$ ). In each case the values between  $1 M_{\odot}$  and  $0.60m_{\text{upper}}$  are plotted. See the electronic version of the journal for a color version of this figure.

easy to see that a direct application of main-sequence fitting to a  $U - V$  vs.  $V$  diagram would lead to an overestimation of the distance, because for a fixed value of  $U - V$  there should be more stars close to the equal-mass binary sequence than to the main sequence itself. Note that this effect should be significantly smaller for older clusters because the binary fraction is lower there, as it is indeed observed for globular clusters (see e.g. Sollima et al. 2007). Spectroscopy can partially resolve the problem by detecting blended spectra or radial velocity variations but from Fig. 1 we can see that it should be also possible to correct for the effect by considering that there is an intrinsic spread in the observed color-magnitude diagram due to binarity (besides the ones due to differential extinction and foreground/background contamination).

## 2.2. Experiment 2: Chance superpositions of single stars

In the second experiment I model the effect of chance superpositions between single (not binary) stars within the observed clusters. Such a simulation introduces additional complications that are detector- and observation-dependent because now we have to deal with a continuous spatial distribution of stars along a 2-D detector. In other words, the observed luminosity function depends not only on the intrinsic properties of the cluster (e.g. its internal structure) but also on the the relative pixel and point-spread function (PSF) sizes, Poisson statistics, and the ability of the detector and the finding algorithm to differentiate between single- and multiple- point sources of diverse  $\Delta m$ . Given those considerations, the goal in this case is to obtain a toy model that allows us to approximately quantify the effect for a given region of a cluster in order to test the magnitude of the effect.

The combination rules in this case are:

1. The light from a given star falls in a single pixel (the *fat pixel approximation*).
2. The initial cluster is built by generating a fine grid in  $U - V$  and  $V$  and assigning to each point a value of  $g_{1s}(U - V, V)$  integrated over the size of the bin. Since  $g_{1s}(U - V, V)$  is zero outside the 1-million year isochrone, most points in the grid have no stars. The initial cluster is then defined by the non-zero values of  $g_{1s}(U - V, V)$ . As with the previous experiment, we consider the two cases of a Kroupa and a top-heavy IMF.
3.  $g_{2s}(U - V, V)$  is a color-magnitude function that describes a cluster with two single stars in each pixel which are randomly paired. I generate it by convolving  $g_{1s}(U - V, V)$  with itself and assigning the result of each pair to the closest value in the  $(U - V, V)$

grid<sup>11</sup>. Note that  $g_{2s}(U - V, V)$  does not take into consideration Poisson statistics for the stellar distribution among pixels but instead considers that each pixel contains exactly two stars.

4.  $g_{4s}(U - V, V)$  is generated by convolving  $g_{2s}(U - V, V)$  with itself, and in general,  $g_{2^n s}(U - V, V)$  is generated by convolving  $g_{2^{n-1}s}(U - V, V)$  with itself. In this paper I generate the color-magnitude functions up to  $n = 11$  i.e.  $g_{2048s}(U - V, V)$ .

Those rules should be able to simulate the general behavior of the observed color-magnitude diagram as the intrinsic stellar density or the cluster distance increases. However, there are three caveats to its direct application. The first one is that a comparison with a real case should always consider the possible additional effect of Poisson fluctuations, especially when the number of superimposed stars  $N_{\text{sup}} = 2^n$  is small. One way to do this if the expected average number of stars per pixel,  $N_{\text{px}}$ , falls between  $2^{n-1}$  and  $2^n$  would be to consider both of those cases as possible. The second caveat is that the fat pixel approximation is not valid for a well-sampled detector (PSF size several times larger than the pixel size), so an effective pixel size has to be defined by calculating the area of influence of a star i.e. the region where the presence of a star does not allow a second star to be detected but instead the fluxes from both are merged. Such an effective pixel size is in reality  $\Delta m$ -dependent so an average effective pixel size should be calculated. Also, the precise flux derived depends on the photometric technique (PSF fitting or aperture photometry) and the algorithm details. Once again, I stress that the purpose of this experiment is not to find the exact correction required to account for chance superpositions but rather to develop a toy model that would allow the observer to roughly quantify the effect. The third caveat is that all stars are assumed to be single. This last caveat will be addressed by the third experiment.

Six of the resulting full color-magnitude density functions,  $g_{2^n s}(U - V, V)$ , are shown in Fig. 4 for  $n = 1, 4, 7$  and the two cases (Kroupa and top heavy). The top left corner (where massive stars are located) of all the functions is shown in Figs. 5 (Kroupa) and 6 (top heavy). As was the case in experiment 1,  $g_{2^n s}(U - V, V)$  is zero nearly everywhere in the color-magnitude diagram except in a narrow band. The band widens up until  $n = 8$  and then narrows down from that point onwards. At the same time, the lower end of the band starts climbing up the vertical coordinate starting at  $n = 1$ . The top end starts climbing up at a lower pace but then picks up speed around  $n = 8$ . The progression of both ends is faster for the top-heavy case than for the Kroupa case. For the final  $n = 11$  value the resulting Hess-diagram has been compressed to a well-defined narrow peak in the  $U - V$  vs.  $V$  color

---

<sup>11</sup>As previously noted, special care was taken to avoid roundoff errors.

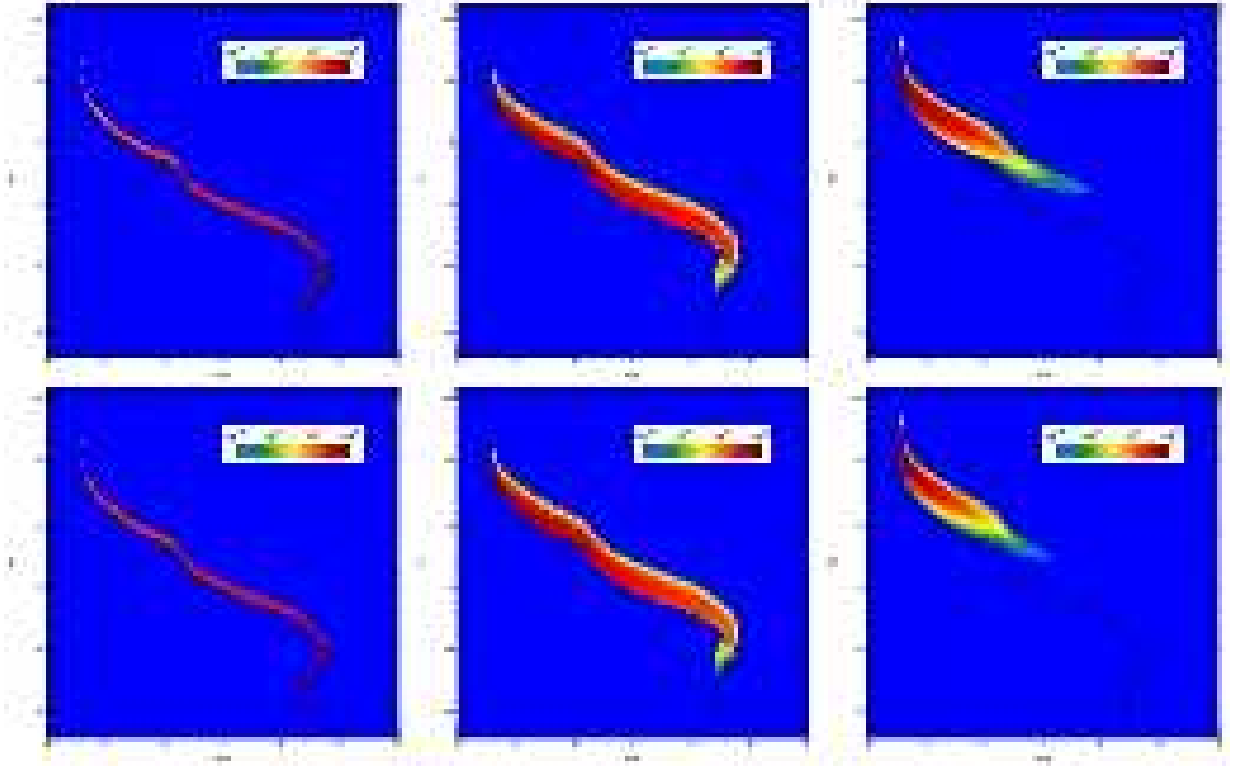


Fig. 4.— Color-magnitude density functions  $g_{2s}(U - V, V)$  (left),  $g_{16s}(U - V, V)$  (center), and  $g_{128s}(U - V, V)$  (right) for the Kroupa (top row) and top-heavy (bottom row) cases of experiment 2 (chance superpositions of single stars) shown as Hess diagrams. The thick black line shows the position of the 1 million year isochrone. The function scaling is logarithmic and the normalization is arbitrary. See the author’s web site <http://www.iaa.es/~jmaiz> for animated gifs showing all the color-magnitude functions  $g_{2^n s}(U - V, V)$  from  $n = 0$  to  $n = 11$ . See the electronic version of the journal for a color version of this figure.



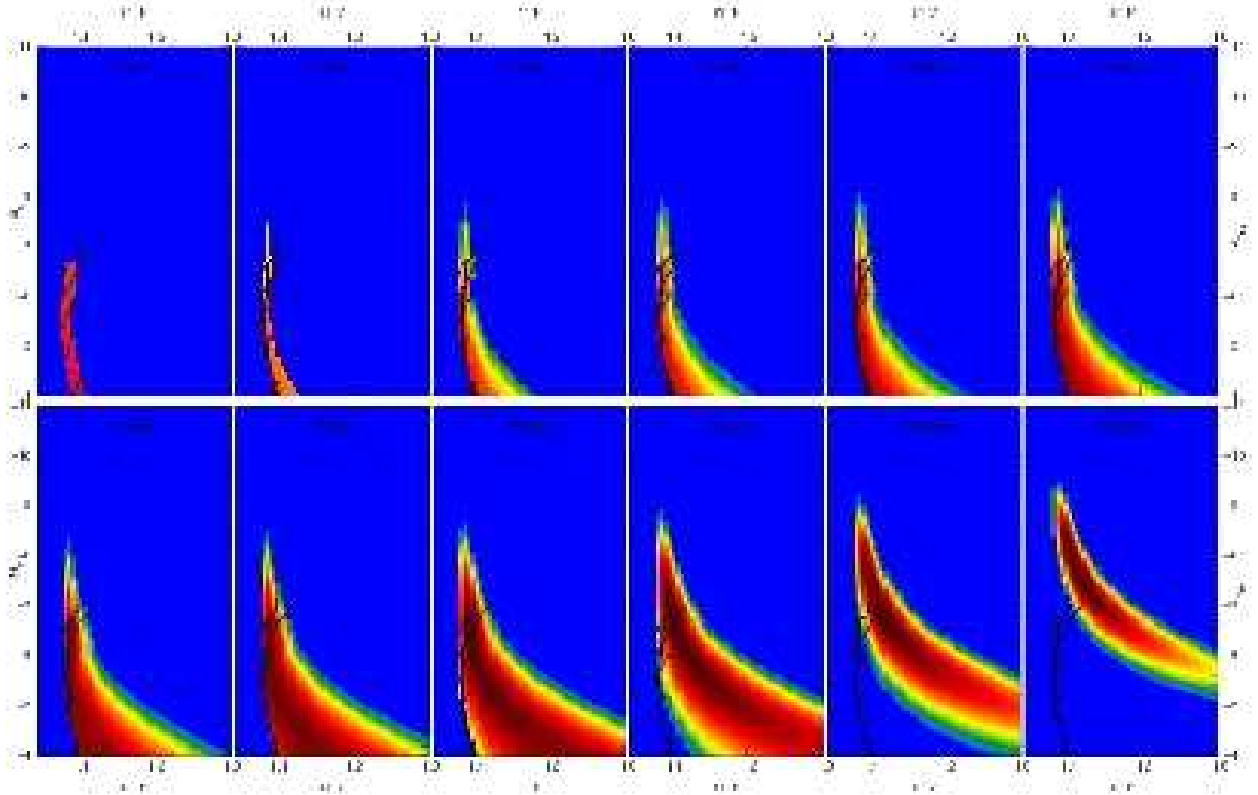


Fig. 5.— Top left corner of the color-magnitude density functions  $g_{2n_s}(U - V, V)$  with  $n = 0, 11$  for the Kroupa case of experiment 2 (chance superpositions of single stars) shown as Hess diagrams. The  $n = 0$  case has been smoothed in order to allow it to show some extent perpendicular to the 1 million year isochrone. The thick black line shows the position of the 1 million year isochrone and the thin lines the evolutionary tracks between 0 and 2 million years for the initial masses of 25, 40, 60, 85, and 120  $M_\odot$ . The function scaling is logarithmic and the normalization is arbitrary. See the electronic version of the journal for a color version of this figure.

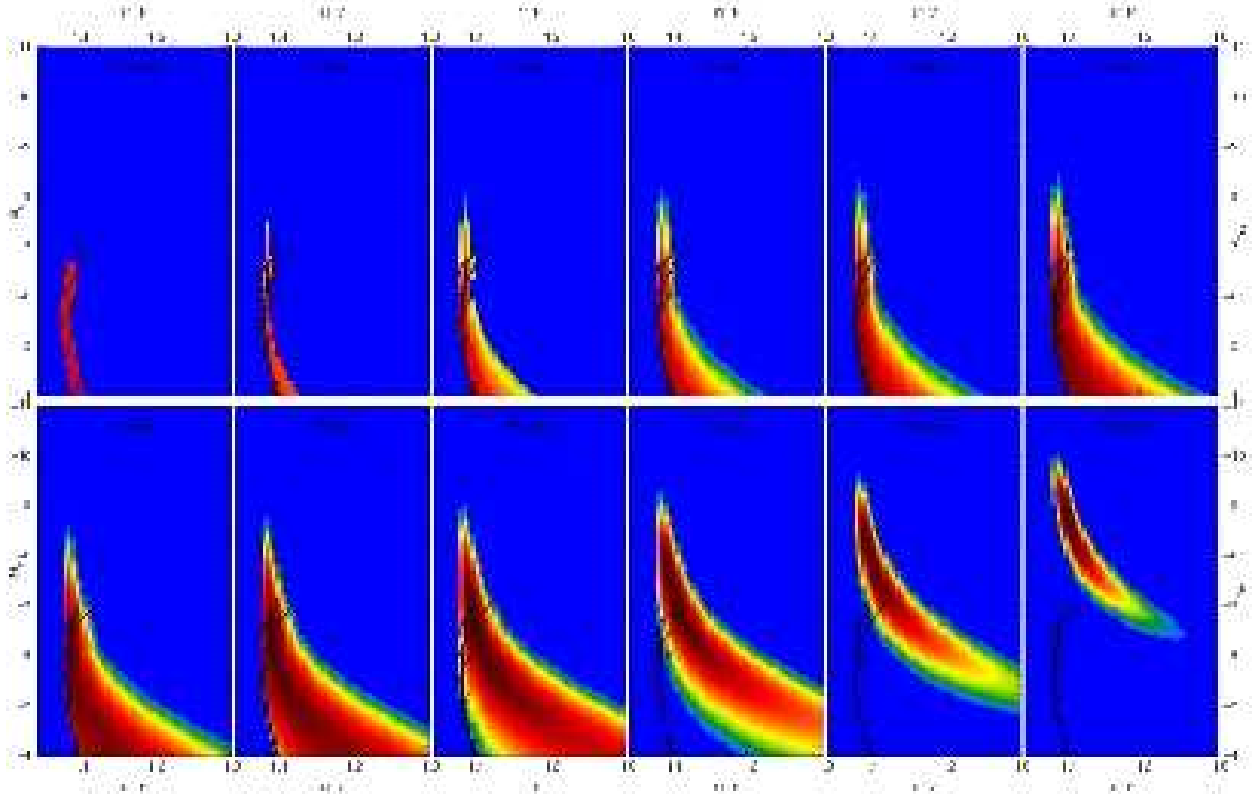


Fig. 6.— Top left corner of the color-magnitude density functions  $g_{2n_s}(U - V, V)$  with  $n = 0, 11$  for the top-heavy case of experiment 2 (chance superpositions of single stars) shown as Hess diagrams. The  $n = 0$  case has been smoothed in order to allow it to show some extent perpendicular to the 1 million year isochrone. The thick black line shows the position of the 1 million year isochrone and the thin lines the evolutionary tracks between 0 and 2 million years for the initial masses of 25, 40, 60, 85, and 120  $M_\odot$ . The function scaling is logarithmic and the normalization is arbitrary. See the electronic version of the journal for a color version of this figure.

diagram: the distribution is completely contained in the last plot of the top-heavy case of Fig. 6 and almost so for the Kroupa case of Fig. 5.

Figures 4, 5, and 6 indicate that, as crowding becomes more of an issue, we progressively lose the ability to detect low-mass stars. Once a certain threshold has been attained, high-mass stars also become significantly affected by crowding. However, one should be careful in overinterpreting those Hess diagrams as color-magnitude probability distributions for the observed population of points source in a given cluster because of the fat pixel assumption. The lower end of the observed band represents in reality those pixels which detection algorithms would simply classify as background. Therefore, a more realistic interpretation of the Hess diagrams would be that the observed point source population measured by assuming a zero background (or calculating it outside the cluster boundaries) is extracted from the top part of the 2-D function given by  $g_{2n_s}(U - V, V)$  and that the lower part represents the unobserved part of the population. The limit between the two regions is defined by the characteristics of the detector and the observations.

An interesting alternative interpretation of Figs. 4, 5, and 6 is that they represent the probability distribution for a cluster with  $2^n$  stars, with the extension in  $U - V$  and  $V$  indicating the result of stochastic effects in drawing the given number of stars from an IMF. I will not explore this interpretation any further in this article; the reader is referred to Cerviño & Luridiana (2006) for more details.

It is also useful to compare the results from  $g_{1b}$  (first experiment) and  $g_{2s}$  (second experiments)<sup>12</sup>. Both functions represent the combination of two stars but with an important difference: in the first case the pairing assumes a flat mass-ratio distribution while in the second case the pairing is random. The different combination rules manifest themselves in the slope that is obtained when plotting  $g_{1b}$  or  $g_{2s}$  as a function of  $V$  for a fixed  $U - V$ . For most values of  $U - V$  in the first case the function increases towards lower values of  $V$  (higher luminosities) while in the second one the behavior is the opposite. The reason is that for random pairing, once an  $m_1$  is drawn in the middle or upper main sequence, chances are that  $m_2$  will be significantly lower. On the other hand, for a flat mass-ratio distribution one gets a larger contribution from stars with  $m_2$  only slightly lower than  $m_1$ , thus tilting the balance at a fixed  $U - V$  towards systems with near-equal mass ratios.

The calculated AMFs for the Kroupa and top-heavy cases are shown in Fig. 7 along with the original IMFs. The overall behavior in both cases again being similar: as the number of stars increases, the left extreme of the AMF moves towards the right in approximately equal amounts in  $\log m$  for each step in  $n$ . The right extreme has a different behavior: the

---

<sup>12</sup>Note that the function scaling in Figs. 1 and 4 is different.

Table 1. Apparent ratios between the number of objects above  $120 M_{\odot}$  and the number in different mass ranges for the two cases of the first experiment.

Mass range $M_{\odot}$	Kroupa real IMF	Top-heavy real IMF
All	$7.873 \cdot 10^{-5}$	$3.639 \cdot 10^{-4}$
1 – 120	$6.661 \cdot 10^{-4}$	$2.246 \cdot 10^{-3}$
3 – 120	$2.835 \cdot 10^{-3}$	$7.142 \cdot 10^{-3}$
5 – 120	$5.941 \cdot 10^{-3}$	$1.294 \cdot 10^{-2}$
8 – 120	$1.164 \cdot 10^{-2}$	$2.225 \cdot 10^{-2}$
15 – 120	$2.921 \cdot 10^{-2}$	$4.726 \cdot 10^{-2}$
25 – 120	$6.206 \cdot 10^{-2}$	$8.895 \cdot 10^{-2}$
40 – 120	$1.284 \cdot 10^{-1}$	$1.662 \cdot 10^{-1}$
60 – 120	$2.656 \cdot 10^{-1}$	$3.163 \cdot 10^{-1}$

Table 2. Apparent ratios between the number of objects above  $120 M_{\odot}$  and the total number of objects for the second (single stars) and third (binaries) experiments.

# of objects	Kroupa singles	Top-heavy singles	Kroupa binaries	Top-heavy binaries
1	$0.000 \cdot 10^{+0}$	$0.000 \cdot 10^{+0}$	$7.873 \cdot 10^{-5}$	$3.639 \cdot 10^{-4}$
2	$2.080 \cdot 10^{-7}$	$3.331 \cdot 10^{-6}$	$1.913 \cdot 10^{-4}$	$8.708 \cdot 10^{-4}$
4	$1.027 \cdot 10^{-6}$	$1.582 \cdot 10^{-5}$	$4.458 \cdot 10^{-4}$	$1.988 \cdot 10^{-3}$
8	$4.829 \cdot 10^{-6}$	$7.101 \cdot 10^{-5}$	$1.033 \cdot 10^{-3}$	$4.552 \cdot 10^{-3}$
16	$2.485 \cdot 10^{-5}$	$3.552 \cdot 10^{-4}$	$2.469 \cdot 10^{-3}$	$1.082 \cdot 10^{-2}$
32	$1.422 \cdot 10^{-4}$	$1.977 \cdot 10^{-3}$	$6.209 \cdot 10^{-3}$	$2.703 \cdot 10^{-2}$
64	$9.067 \cdot 10^{-4}$	$1.155 \cdot 10^{-2}$	$1.646 \cdot 10^{-2}$	$7.090 \cdot 10^{-2}$
128	$6.040 \cdot 10^{-3}$	$6.253 \cdot 10^{-2}$	$4.626 \cdot 10^{-2}$	$1.948 \cdot 10^{-1}$
256	$3.697 \cdot 10^{-2}$	$2.790 \cdot 10^{-1}$	$1.385 \cdot 10^{-1}$	$5.045 \cdot 10^{-1}$
512	$1.907 \cdot 10^{-1}$	$7.765 \cdot 10^{-1}$	$4.079 \cdot 10^{-1}$	$9.118 \cdot 10^{-1}$
1024	$6.667 \cdot 10^{-1}$	$9.979 \cdot 10^{-1}$	$8.684 \cdot 10^{-1}$	$9.998 \cdot 10^{-1}$
2048	$9.944 \cdot 10^{-1}$	$1.000 \cdot 10^{+0}$	$9.997 \cdot 10^{-1}$	$1.000 \cdot 10^{+0}$

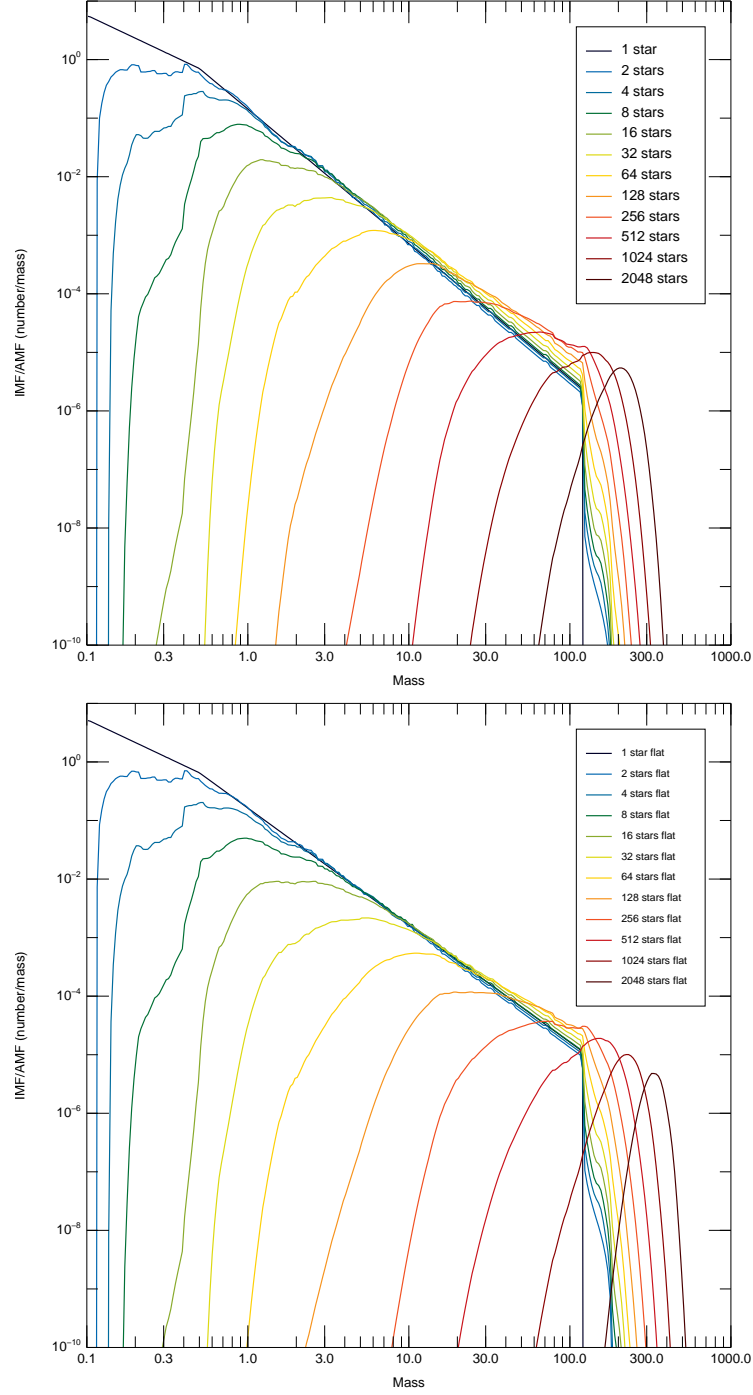


Fig. 7.— IMF and AMFs for experiment 2 (chance superpositions of single stars). The top panel shows the Kroupa case and the bottom panel the top-heavy case. The mass is expressed in solar units. The IMF is normalized to 1.0 and the AMFs to  $2^{-n}$ .

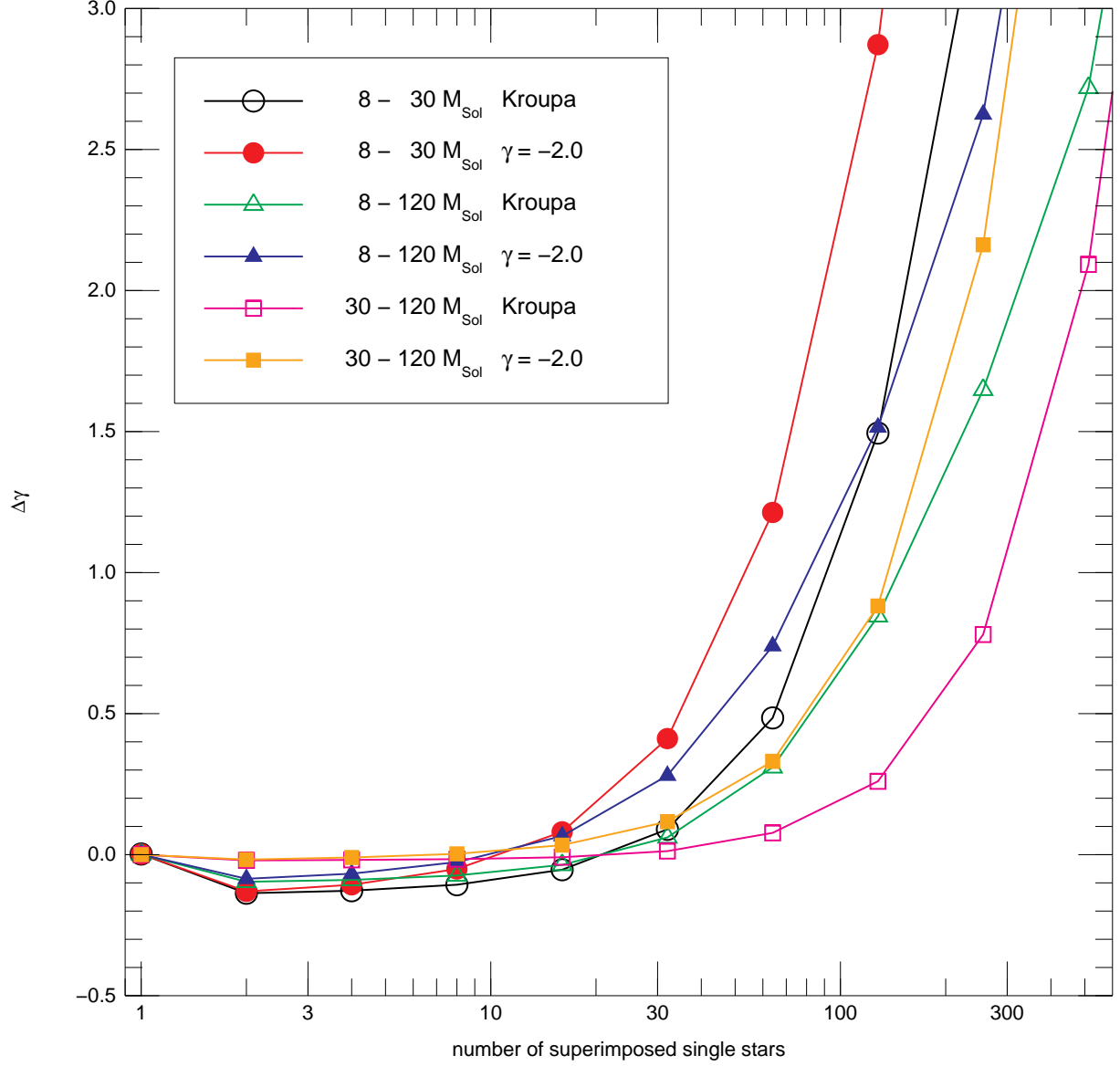


Fig. 8.— Slope change introduced by chance superpositions of single stars (second experiment) as a function of the number of superimposed single stars for the two IMF cases and for three different mass ranges. See the electronic version of the journal for a color version of this figure.

population of AUMSs initially appears only as a weak tail and it is only when  $n = 7 - 8$  that a significant number is built up. From then on, the right extreme of the AMF picks up speed and starts moving towards the right, though at a lower pace than the left extreme. As a consequence, the distribution narrows in  $\log m$ . The narrowing process also affects the overall shape of the distribution, which for  $n = 11$  is already quite similar to a log-normal (especially for the top-heavy case).

Table 2 lists the fraction of objects with apparent masses above  $m_{\max} = 120 M_{\odot}$  for both the Kroupa (second column) and top-heavy cases (third column) as a function of  $N_{\text{sup}}$ . The fraction is highly dependent on the IMF slope, with the top-heavy case showing values an order of magnitude above the Kroupa case until the point where the value becomes close to unity for the top-heavy case ( $n \approx 9$ ). Such a dependence is not an unexpected behavior, because even a small change in  $\gamma$  is sufficient to produce a large variation in the ratio of stars with masses around  $100 M_{\odot}$  to low-mass stars in the real IMF (compare e.g. the two panels in Fig. 2). As also expected, flat-mass ratio binaries are significantly more efficient than chance superpositions in creating a population of AUMSs:  $\approx 32$  superimposed stars are required to create the same number of those stars as those created by a single binary for the Kroupa case (the number is slightly lower for the top-heavy case).

Figure 8 plots  $\Delta\gamma$  the change in MF slope as a function of  $N_{\text{sup}}$  for three mass ranges. Three regimes can be distinguished. For low  $N_{\text{sup}}$ , the effect in  $\Delta\gamma$  is small and in most cases implies a slight steepening of order 0.1. For intermediate values,  $\Delta\gamma$  starts to increase (the mass function becomes flatter) but the effect remains small and should be correctable. Finally, for large  $N_{\text{sup}}$ ,  $\Delta\gamma$  becomes so large that no realistic correction is possible.

### 2.3. Experiment 3: Chance superpositions of binaries

The third experiment is a combination of the previous two. I start with the color-magnitude generated in the first experiment for flat mass-ratio binaries,  $g_{1b}(U - V, V)$ , and I convolve it with itself to derive  $g_{2b}(U - V, V)$ .  $g_{4b}(U - V, V)$  is then generated by convolving  $g_{2s}(U - V, V)$  with itself and the process is repeated until  $n = 11$  i.e.  $g_{2048b}(U - V, V)$ . This experiment should provide the most realistic representation of the observed color-magnitude density function and AMF of a distant cluster, always keeping in mind the first two caveats previously discussed.

As I did for the second experiment, I show six of the resulting full color-magnitude density functions,  $g_{2^n b}(U - V, V)$  in Fig. 9 for  $n = 1, 4, 7$  and the two cases (Kroupa and top heavy). The top left corner (where massive stars are located) of all the functions is shown in

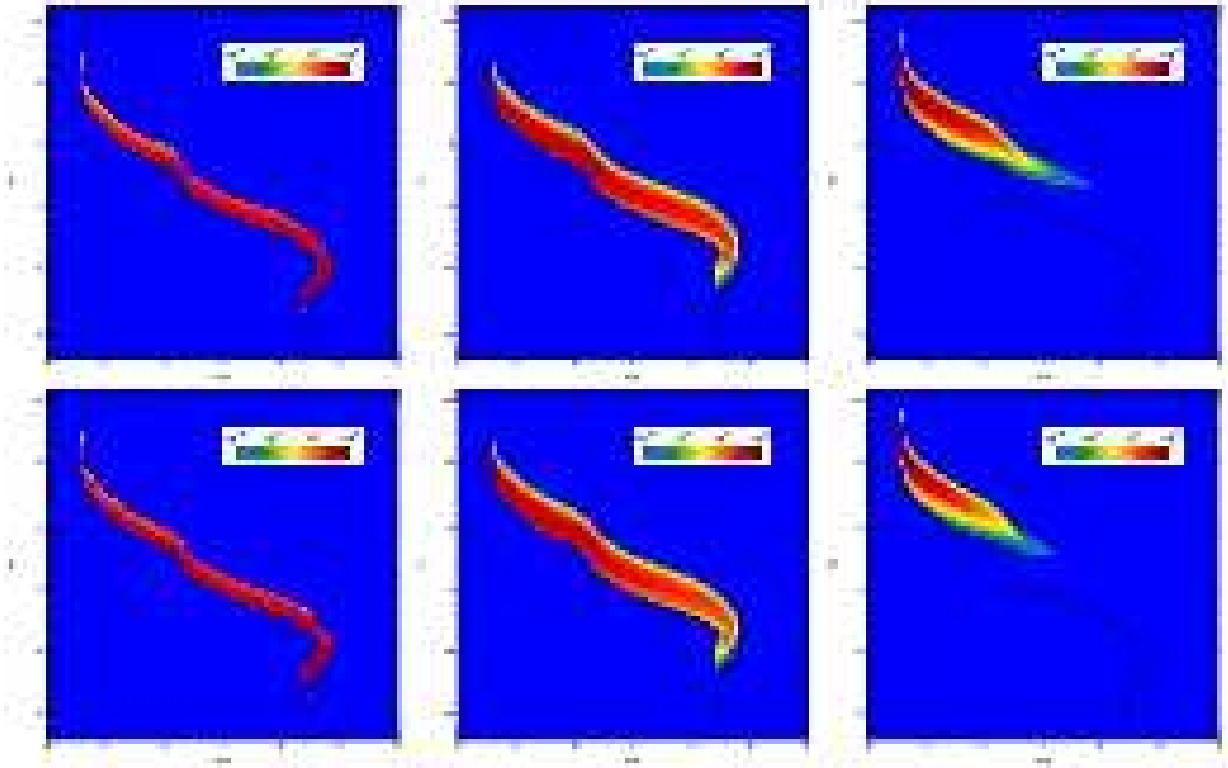


Fig. 9.— Color-magnitude density functions  $g_{2b}(U - V, V)$  (left),  $g_{16b}(U - V, V)$  (center), and  $g_{128b}(U - V, V)$  (right) for the Kroupa (top row) and top-heavy (bottom row) cases of experiment 3 (chance superpositions of binaries) shown as Hess diagrams. The thick black line shows the position of the 1 million year isochrone. The function scaling is logarithmic and the normalization is arbitrary. See the author’s web site <http://www.iaa.es/~jmaiz> for animated gifs showing all the color-magnitude functions  $g_{2^n b}(U - V, V)$  from  $n = 0$  to  $n = 11$ . See the electronic version of the journal for a color version of this figure.



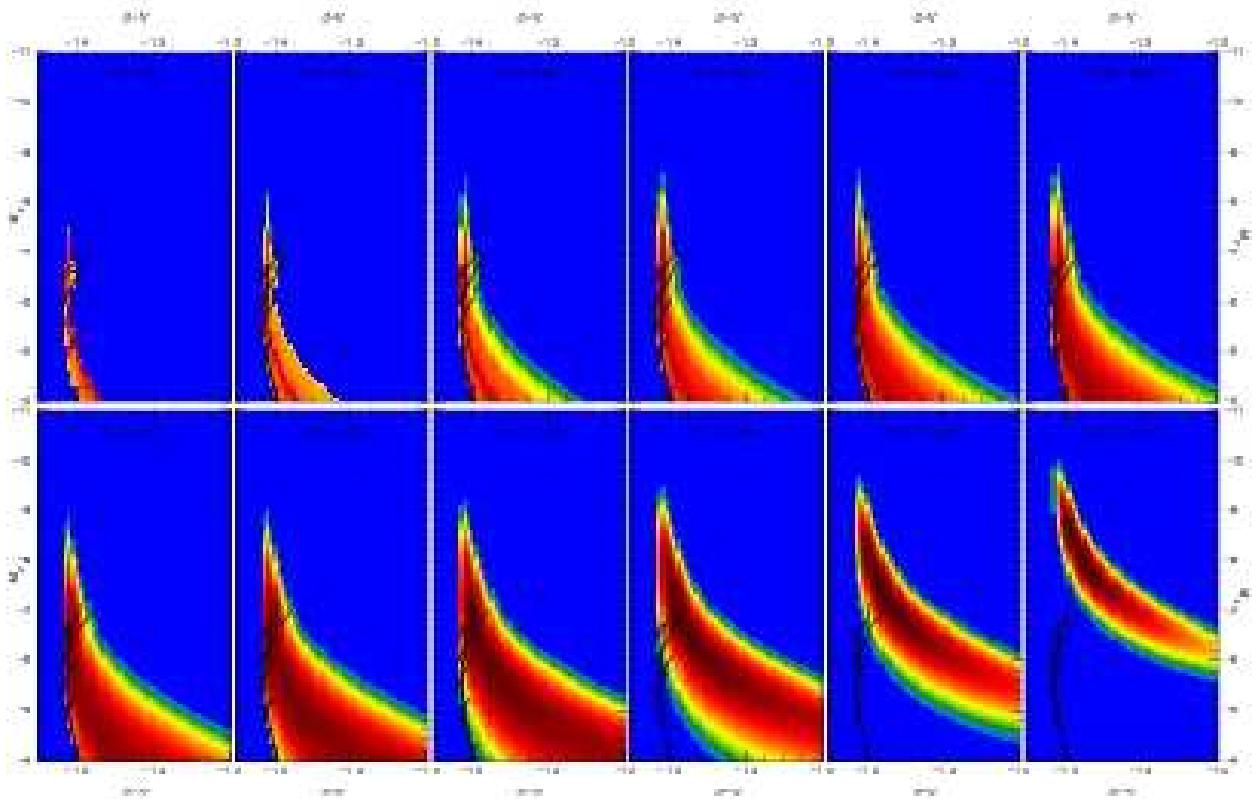


Fig. 10.— Top left corner of the color-magnitude density functions  $g_{2n_b}(U - V, V)$  with  $n = 0, 11$  for the Kroupa case of experiment 3 (chance superpositions of binaries) shown as Hess diagrams. The  $n = 0$  case has been smoothed in order to allow it to show some extent perpendicular to the 1 million year isochrone. The thick black line shows the position of the 1 million year isochrone and the thin lines the evolutionary tracks between 0 and 2 million years for the initial masses of 25, 40, 60, 85, and 120  $M_\odot$ . The function scaling is logarithmic and the normalization is arbitrary. See the electronic version of the journal for a color version of this figure.

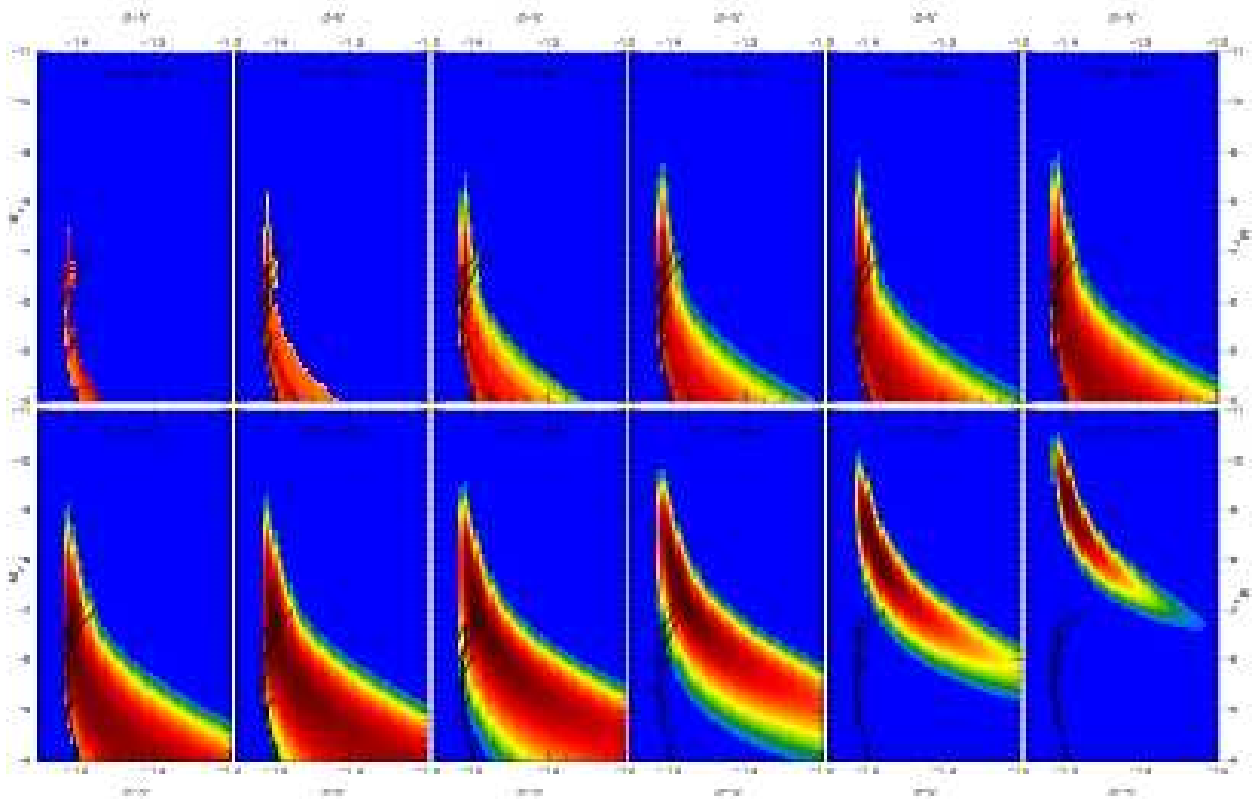


Fig. 11.— Top left corner of the color-magnitude density functions  $g_{2n_b}(U - V, V)$  with  $n = 0, 11$  for the top-heavy case of experiment 3 (chance superpositions of binaries) shown as Hess diagrams. The  $n = 0$  case has been smoothed in order to allow it to show some extent perpendicular to the 1 million year isochrone. The thick black line shows the position of the 1 million year isochrone and the thin lines the evolutionary tracks between 0 and 2 million years for the initial masses of 25, 40, 60, 85, and 120  $M_\odot$ . The function scaling is logarithmic and the normalization is arbitrary. See the electronic version of the journal for a color version of this figure.

Figs. 10 (Kroupa) and 11 (top heavy). Those three figures are quite similar to the equivalent ones for the second experiment. The most prominent differences are: [a] the non-zero regions of  $g_{2^n_b}(U - V, V)$  are more extended in their short direction (in the diagrams, from the lower left to the upper right) compared to the non-zero regions of  $g_{2^n_s}(U - V, V)$  due to the additional widening introduced by binaries; and [b] the extension of  $g_{2^n_b}(U - V, V)$  in its long direction (from the lower right to the upper left) is similar to that of  $g_{2^n_s}(U - V, V)$  but it is slightly displaced towards lower magnitudes (higher luminosities) due to the additional factor of two in the number of superimposed objects. The latter effect is especially noticeable for large values of  $n$  (compare the lower right panels of Figs. 5 and 10 or those of Figs. 6 and 11). Note, however, that a comparison of the two experiments assuming the same number of superimposed individual stars implies using  $g_{2^n_s}(U - V, V)$  and  $g_{2^{n-1}_b}(U - V, V)$ . If the comparison is done in that way one finds that for large  $n$  the top parts of the non-zero regions of the two functions end near a similar value (with the  $g_{2^{n-1}_b}(U - V, V)$  one only slightly higher in luminosity) and that the low-luminosity tail of  $g_{2^{n-1}_b}(U - V, V)$  is significantly more extended than that of  $g_{2^n_s}(U - V, V)$ .

The calculated AMFs for the third experiment are shown in Fig. 12, with the overall behavior in both cases being similar to the equivalent ones for the second experiment. A more detailed comparison shows that for low values of  $n$  the behavior beyond  $m_{\max}$  is quite different: both experiments start by developing a tail from their  $n = 0$  case but since each initial distribution has a very different apparent upper mass limit (for experiment 2 it is the real  $m_{\max}$  while for experiment 3 it is  $m_{\max,1b}$ ) the fraction of stars above the limit starts from a much higher value for experiment 3 and grows at a significantly slower pace (see Table 2). For large values of  $n$  the left side of  $g_{2^{n-1}_b}(U - V, V)$  is quite similar to that of  $g_{2^{n-1}_s}(U - V, V)$  while its right side is similar to  $g_{2^n_s}(U - V, V)$ .

Figure 13 plots the change in MF slope  $\Delta\gamma$  as a function of  $N_{\text{sup}}$  for three mass ranges. The same three regimes as in Fig. 8 can be distinguished. For low  $N_{\text{sup}}$ , the effect in  $\Delta\gamma$  is small and can be approximated by the value derived from the first experiment. For intermediate values,  $\Delta\gamma$  increases moderately (the mass function becomes flatter) and the effect remains correctable. Finally, for large  $N_{\text{sup}}$ ,  $\Delta\gamma$  becomes very large and no realistic correction is possible.

### 3. Sample applications

In this section I apply the results of the experiments above to the IMFs derived from HST observations for two of the best studied massive young clusters in the Local Group, NGC 3603 and R136. In order to do that, two preliminary steps are required:

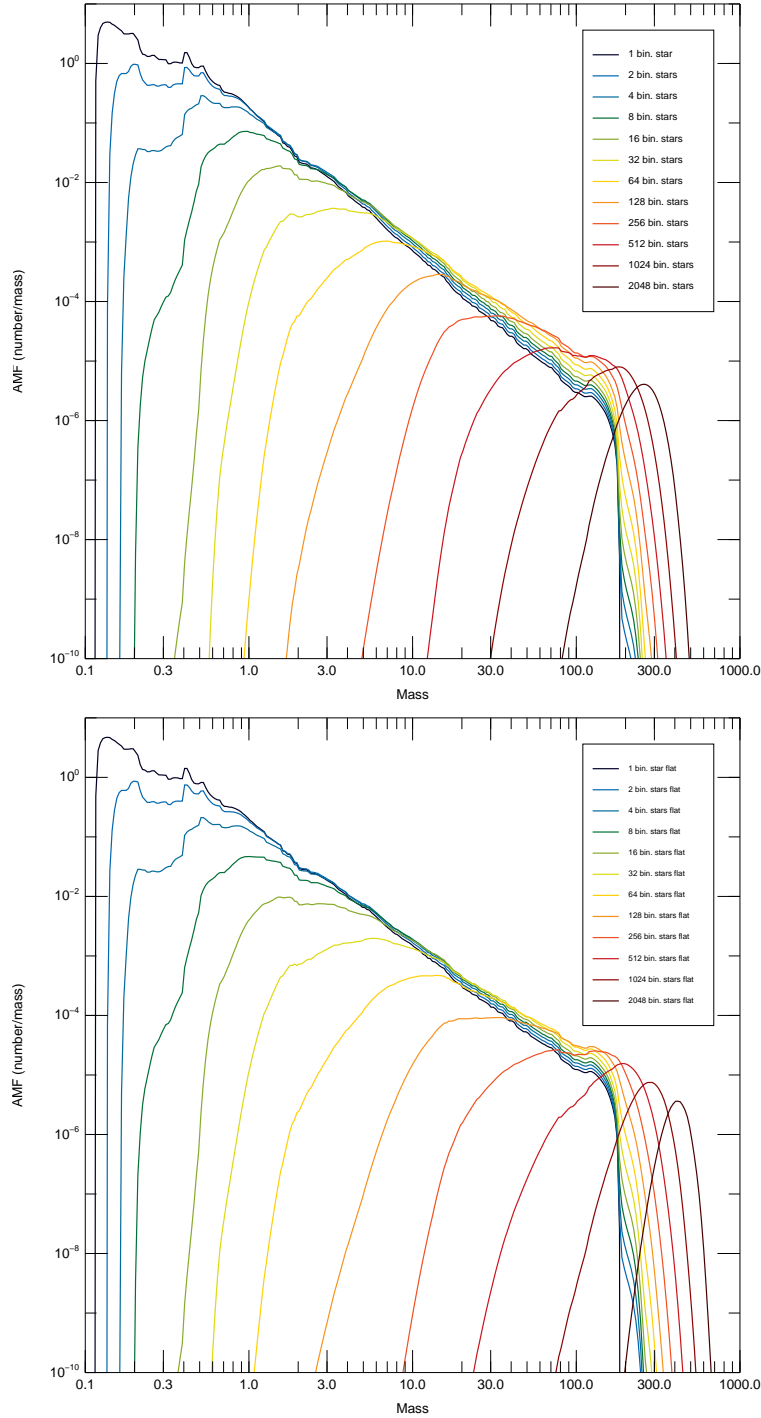


Fig. 12.— AMFs for experiment 3 (chance superpositions of binaries). The top panel shows the Kroupa case and the bottom panel the top-heavy case. The mass is expressed in solar units. All AMFs are normalized to  $2^{-(n+1)}$ .

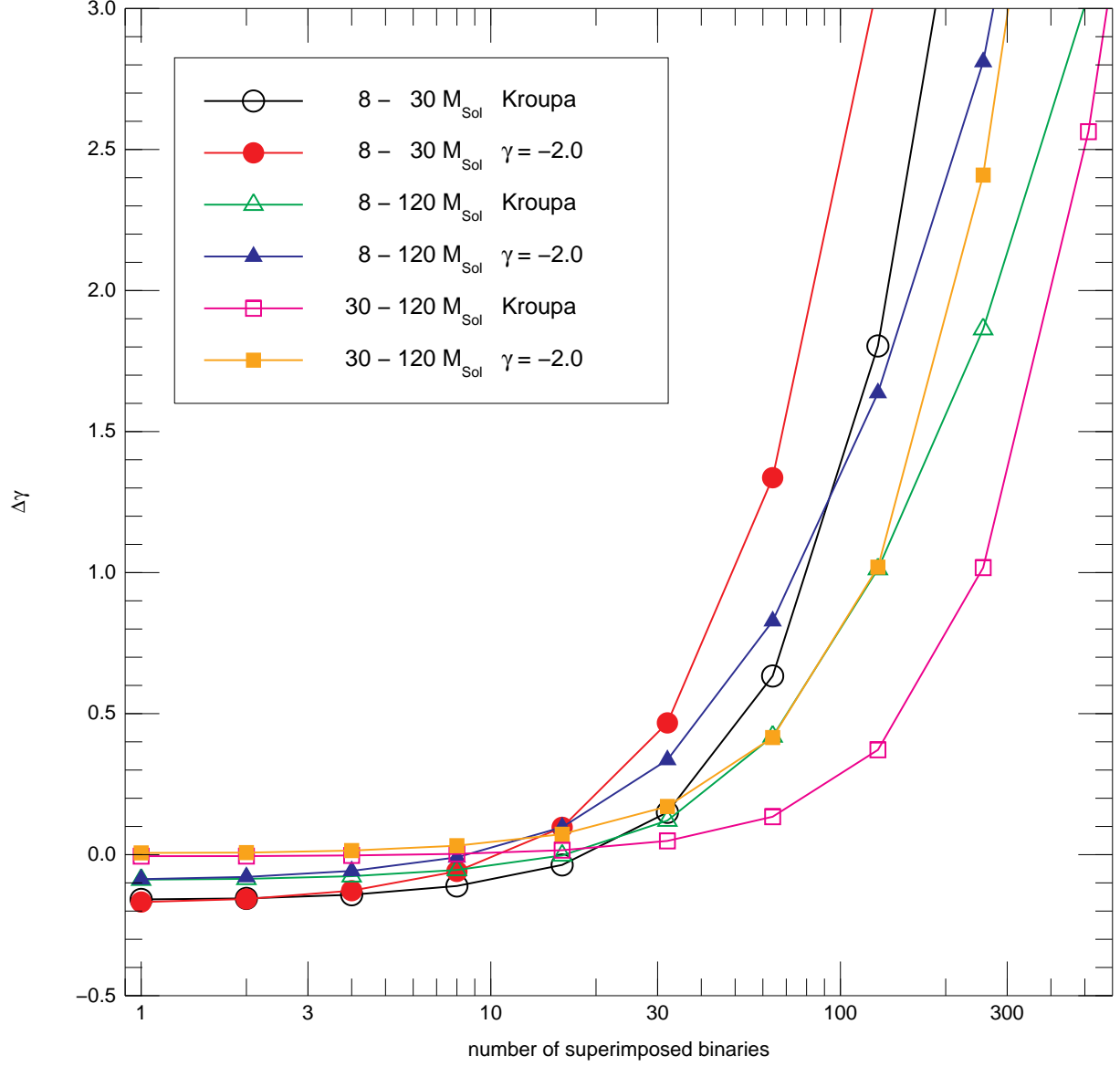


Fig. 13.— Slope change introduced by chance superpositions of binaries (third experiment) as a function of the number of superimposed binaries for the two IMF cases and for three different mass ranges. See the electronic version of the journal for a color version of this figure.

1. Derive the radius of an effective pixel. As previously mentioned, the value depends not only on the detector properties but also on  $\Delta m$ . Indeed, ACS/HRC on HST can separate low  $\Delta m$  objects only 2 pixels apart (Maíz Apellániz et al. 2008a) (effective radius of 1 pixel) but for large  $\Delta m$  the effective radius can grow to 4-5 pixels (similar values apply to the PC of WFPC2). As a compromise, we adopt a value of 2.5 pixels.
2. Determine the average number of stars per effective pixel,  $N_{\text{epx}}$ , given by:

$$N_{\text{epx}} = \left( \frac{d}{10 \text{ pc}} \right)^2 10^{-0.4(m_{V,\text{epx}} - M_{V,1})}. \quad (1)$$

In Eqn. 1,  $d$  is the distance to the object,  $m_{V,\text{epx}}$  is the averaged  $V$ -band extinction-corrected measured magnitude in a single effective pixel, and  $M_{V,1}$  is the absolute magnitude of a “1-star cluster” derived from evolutionary synthesis (calculated by deriving  $M_V$  for a large cluster with e.g.  $N = 10^6$  stars and then adding  $2.5 \log N$ ). If needed,  $V$ -based values can be substituted by those from other passband.

### 3.1. NGC 3603

NGC 3603 is the massive young cluster with the lowest extinction in the Galaxy. Moffat et al. (1994) described it as a Galactic clone of R136 without the halo due to their similarities in age, stellar content, and central density. Note, however, that most of the mass of 30 Doradus is located outside R136, making it significantly more massive than NGC 3603. A study with HST spectroscopy by Drissen et al. (1995), recently extended from the ground by Melena et al. (2007), indicates that NGC 3603 contains the highest concentration of well-classified O2/3 + WNha stars in the Galaxy.

I show in Table 3.1 the literature data for the distance and extinction to the core of NGC 3603. The values for the extinction are quite homogeneous and here we adopt  $A_V = 4.50$ . Also, at the location of the central cluster there is little point-to-point variation in the extinction (Moffat 1983; Melnick et al. 1989; Melena et al. 2007), so the assumption of a constant foreground screen appears reasonable<sup>13</sup>. The disagreement on the distance to NGC 3603 is larger. Different methods and observations yield values between  $\approx 6$  kpc and  $\approx 8$  kpc (see Melena et al. 2007 for a discussion). In order to consider the different possibilities, I adopt three possible distances of 6, 7, and 8 kpc, which I refer to as the short, intermediate, and long distances, respectively. Regarding the age of the core of NGC 3603,

---

<sup>13</sup>Strong extinction variations exist at larger radii but those do not concern us here.

it was previously thought to be  $\approx 3$  million years based on the presence of WR stars but now it is believed that those objects are still in their core hydrogen-burning stage (i.e. they are WNha stars, see e.g. Crowther 2007) and the currently favored age is 1 million years (Stolte et al. 2004; Sung & Bessell 2004), which I adopt.

NGC 3603 was observed with HST/ACS on 29 December 2005 under GO program 10602 using both the WFC and HRC detectors and several filters. Here I use the HRC F550M data, combined with the literature information described above for the distance, extinction, and age, to study the blending effect created by real multiple systems and chance alignments on the NGC 3603 IMF. In a future paper we will use all the data to do a more thorough analysis that will include independent measurements of the distance and extinction. Four F550M exposures of 2 s each were obtained with a dithering pattern that covers the gap produced by the HRC occulting finger. The exposure time was chosen in order to avoid saturation of the brightest stars. MULTIDRIZZLE was used to generate a common geometrically-undistorted cosmic-ray-corrected drizzled (DRZ) frame, see Fig. 14, as well as to clean the individual geometrically-distorted flat-fielded (FLT) frames from cosmic rays and hot pixels.

JMAPHOT, a crowded-field photometry package specifically designed for HST images was used for the data reduction. First, a search is performed in the DRZ frame to find all the sources above a certain S/N threshold. JMAPHOT finds the sources in order from bright to dim and, after each one is found, a model (the drizzled PSF for point sources, simple kernels for extended sources and possible leftover cosmic rays and hot pixels) is subtracted from the data and a correction applied to the weight map before the next source is searched for. This technique allows for the exclusion of false positives caused by complex PSFs with secondary peaks and for the detection of some of the otherwise false negatives close to bright sources. Once a source list is built, the coordinates are transformed back to each of the distorted, cleaned FLT frames and PSF photometry is performed on each one of them. Positions and fluxes of each star are fitted simultaneously; also, stars with close neighbors are grouped together and fitted at the same time. Several passes are performed to eliminate the small contributions from distant stars and to improve the initial PSF model (derived from Anderson & King 2004 with wings from Tiny Tim, Krist 1995) by calculating the PSF residuals. Aperture and charge-transfer efficiency corrections are applied to the flux from each individual FLT frame and the four values are finally combined to derive the observed VEGAMAG magnitude for each object.

Several steps are needed to convert the observed magnitudes into masses. First, F550M values are transformed into the Johnson  $V$  band by adding 0.120 mag, as calculated for the appropriate input SED and extinction using the synthetic photometry package in CHORI-

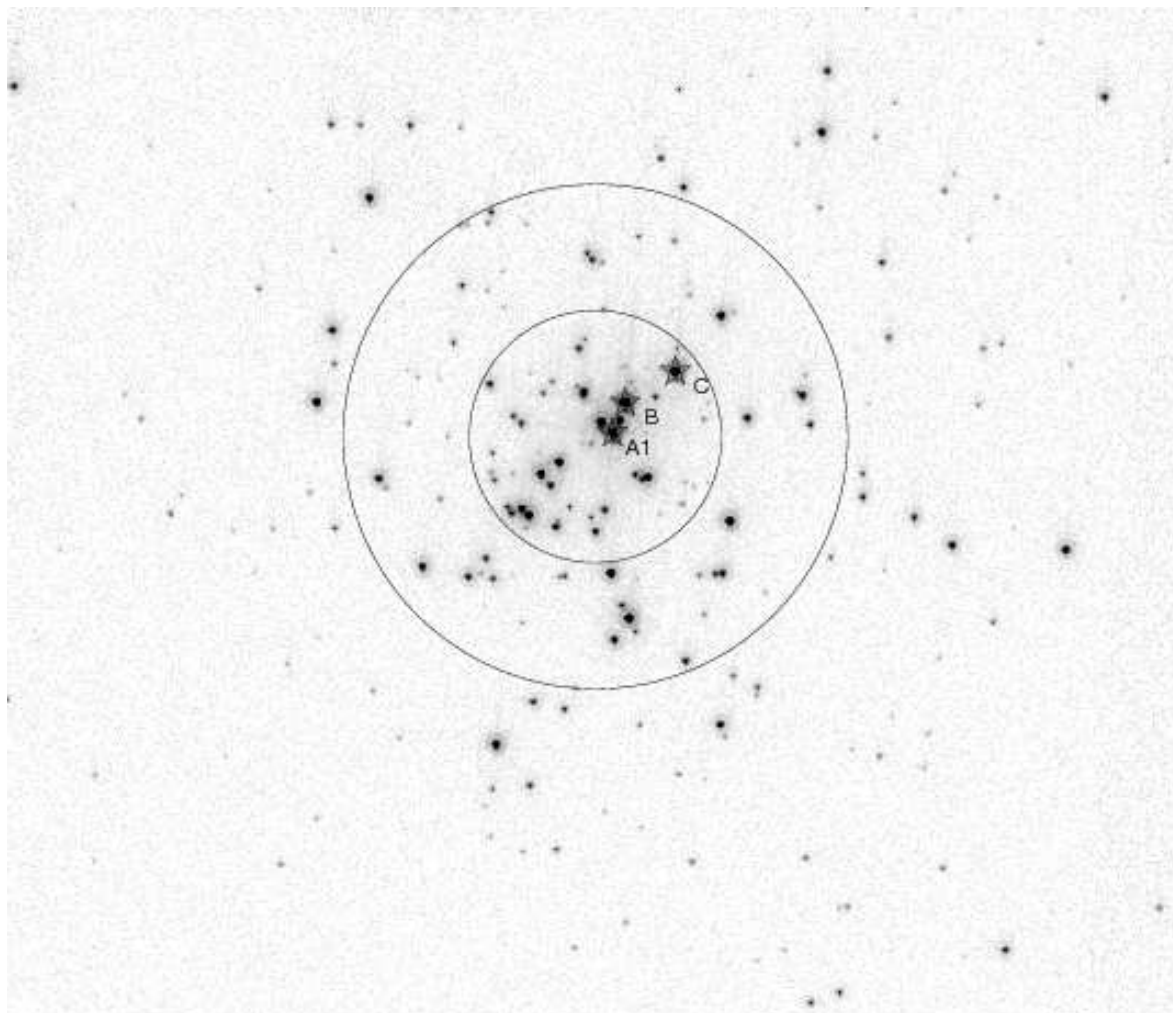


Fig. 14.— ACS/HRC F550M DRZ frame of NGC 3603. The three WNH $\alpha$  objects are marked and circles with radii of 3'' and 6'' centered on the cluster have been drawn. A square-root scale between 0 and 800 counts has been used in order to show both the bright and the dim stars. The pixel size is 0''.025, the field size is 29'.3 $\times$ 25'.4 (1172 px  $\times$  1016 px), and the vertical direction is 124° East of North.



ZOS<sup>14</sup>. Second,  $5 \log d - 5$  is subtracted to obtain the absolute magnitudes  $V$  for each of the short, intermediate, and long distances. Finally, I use  $m(V)$  to obtain the corresponding apparent masses. The first three rows in Table 3.1 give the values I obtain for the three brightest objects in NGC 3603: A1, B, and C.

In order to derive the AMF I first eliminate those objects with observed masses below  $8 M_{\odot}$ . Using such a large cutoff allows us not to worry about incompleteness due to low S/N, since an  $8 M_{\odot}$  isolated star has a S/N of  $\approx 35$  in a single FLT frame and of  $\approx 70$  in the combined DRZ frame<sup>15</sup>. Also, since I want to compare the results with the experiments in the previous section, those stars with apparent masses above  $120 M_{\odot}$  (A1, B, and, for the two longest distances, C) are also excluded i.e. only the  $8\text{--}120 M_{\odot}$  range is used for the power-law fit. No contamination correction is applied given the small size of the field, the high density of stars in the cluster, and that most such objects should be dimmer than the equivalent to the  $8 M_{\odot}$  cutoff. Finally, the AMF is fitted using bins with an equal number of objects, as prescribed in Paper I. Different numbers of bins were tried but the slopes were left essentially unchanged, as expected from the results in that paper. The results for 10 bins are shown in Table 3.1 and plotted in Fig. 15. For comparison purposes, a fit with 10 bins of equal width was also attempted and, as expected, the obtained slopes were significantly different due to the bias inherent in such a method. Also, the measured uncertainties using bins of equal width were a factor of three larger (see Table 3.1). Note that for the three distances  $\gamma_{\text{equal number}}$  is compatible (less than 1 sigma in two cases, less than 1.5 sigmas in the other) with the value we have used for our top-heavy experiments ( $\gamma = -2.0$ )<sup>16</sup>, so that will be the assumed slope for the rest of this subsection.

Finally, to correct for the effects of unresolved binaries and/or chance superpositions, we need to calculate  $N_{\text{epx}}$  using Eqn. 1. With the evolutionary synthesis module of CHORIZOS I obtain that the absolute  $V$  magnitude of a solar-metallicity 1-million-year old top-heavy “1-star cluster” is  $-0.75$ . The other quantity needed is the observed average magnitude in an effective pixel, which will depend on the aperture radius chosen. The DRZ field has a size of  $29''.3 \times 25''.4$  but 69% of the flux is contained within a radius of  $3''$  and 94% within a radius of  $6''$ . Therefore, the area enclosed within those two radii provide reasonable descriptions

---

<sup>14</sup>The value depends on the exact SED and  $A_V$  but the added uncertainty is of the order of only a few thousandths of a magnitude, which is good enough for our purposes.

<sup>15</sup>Note that most incompleteness analyses deal with two different types of non-detections, those due to low S/N of the object and those due to the proximity of bright sources. Since the latter is already taken care of by our experiments, we only need to worry about the former.

<sup>16</sup>Of course, the observed  $\gamma$  is that of the AMF, not the IMF, but, as we will see below, both should be very similar in this case.

Table 3. Distances and extinctions for NGC 3603. The uncertainties shown are standard deviations.

Source	$d$ (kpc)	$A_V$ (mag)
Moffat (1983)	$7.0 \pm 0.5$	$4.46 \pm 0.28$
Melnick et al. (1989)	7.2	$4.47 \pm 0.40$
Eisenhauer et al. (1998)		4.60
de Pree et al. (1999)	$6.1 \pm 0.6$	
Nürnberg et al. (2002)	$7.7 \pm 0.2$	
Stolte et al. (2004)	$6.0 \pm 0.3$	$4.50 \pm 0.60$
Sung & Bessell (2004)	$6.9 \pm 0.6$	4.44
Melena et al. (2007)	7.6	4.66

Table 4. Results for NGC 3603 for the three assumed distances.

Quantity	$d = 6$ kpc	$d = 7$ kpc	$d = 8$ kpc
$M_{A1}$ ( $M_\odot$ )	159	189	217
$M_B$ ( $M_\odot$ )	147	176	203
$M_C$ ( $M_\odot$ )	105	130	152
$\gamma_{\text{equal number}}$	$-1.98 \pm 0.16$	$-1.98 \pm 0.14$	$-1.83 \pm 0.12$
$\gamma_{\text{equal width}}$	$-2.33 \pm 0.49$	$-2.68 \pm 0.42$	$-2.37 \pm 0.39$
$\gamma_{\text{IMF}}$	$-1.90 \pm 0.16$	$-1.90 \pm 0.14$	$-1.74 \pm 0.12$
$N_{\text{epx}} (3'')$	0.64	0.88	1.15
$N_{\text{epx}} (6'')$	0.21	0.29	0.38
$N_{>120M_\odot, 2s}$	0.01	0.01	0.01
$N_{>120M_\odot, 1b}$	2.40	2.83	3.07

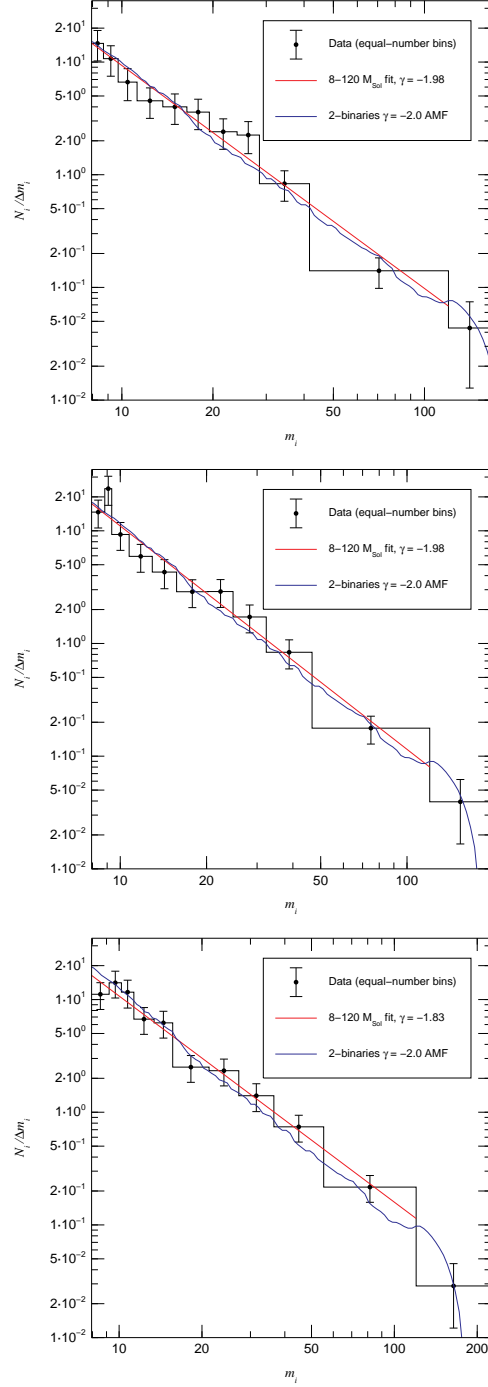


Fig. 15.— AMFs for NGC 3603 assuming a distance of 6.0 kpc (top), 7.0 kpc (middle), and 8.0 kpc (bottom). In each case the data, the power-law fit in the 8-120  $M_\odot$  range, and the top-heavy 2-binaries AMF are shown. Masses are in  $M_\odot$ . See the electronic version of the journal for a color version of this figure.

of the center of NGC 3603 and of the region that contains most of the light from the core, respectively. The resulting  $N_{\text{epx}}$  are shown in Table 3.1. Depending on the distance and radius selected, I find that, on average, each point source in NGC 3603 contains at most 1.15 individual stars due to chance superpositions with the assumption that all systems are single and not unresolved binaries. Therefore, chance superpositions are not an important issue for the NGC 3603 HRC data and, indeed, most effective pixels should be empty. Of course, if most point sources are binaries the results of the first experiment are still relevant.

What do our experiments tell us about the corrections required to analyze the AMF in terms of the real IMF of NGC 3603? With the observed values of  $N_{\text{epx}}$ ,  $f_{a,1b}$  (1 binary) should be the closest approximation to reality if indeed most stars are binaries (note that for binaries the values of  $N_{\text{epx}}$  have to be reduced by a factor of two and that those values represent the average number of binaries per effective pixel). As a comparison, I also discuss the case of  $f_{a,2s}$  (2 single stars), which is less realistic but is the closest choice among the results of the second experiment. Regarding  $\Delta\gamma$ , both AMFs indicate that the measured slope for the range 8-120  $M_{\odot}$  will be slightly steeper than the real IMF ( $\Delta\gamma = -0.086 f_{a,2s}$  and by  $\Delta\gamma = -0.087$  for  $f_{a,1b}$ ). Applying the correction  $-\Delta\gamma$  we arrive at the final values for the IMF slope,  $\gamma_{\text{IMF}}$ , shown in Table 3.1. For the short and intermediate distances, I obtain a slope close to the  $-2.0$  while for the long distance the slope is slightly steeper. The values are in good agreement with the recent result by Stolte et al. (2006), who measured an IMF for NGC 3603 with  $\gamma = -1.89 \pm 0.14$  between  $7''$  and  $20''$  (note, however, that their  $m_{\text{lower}}$  is significantly lower than 8  $M_{\odot}$ ).

The result is different for the expected number of ultramassive objects,  $N_{>120M_{\odot}}$ , shown in Table 3.1. For the single-star case, the expected number is almost zero. For the binary case, the predicted numbers are  $\sim 2$  for the short distance and  $\sim 3$  for the intermediate and long distances. In other words, *if the real stellar upper mass limit is 120  $M_{\odot}$ , we would expect two or three stars with apparent masses beyond that limit if most objects are unresolved binaries* and that is precisely the number that is observed.

What else do we know about A1, B, and C, the three brightest point sources in NGC 3603? Drissen et al. (1995) identified them as the source of the Wolf-Rayet part of the composite WR+O integrated spectrum of the core, as had been already partially suggested by Walborn (1973). Since hydrogen is present and there is intrinsic absorption in the high-order Balmer lines, they are classified as WN6ha, implying that they are the more luminous and massive cousins of the O3 stars in their immediate vicinity. Therefore, from the point of view of their spectral classification they are good candidates to have masses above 120  $M_{\odot}$  if such stars really exist. However, it is also possible that they are unresolved multiple systems composed of individual stars with masses in the range 70-120  $M_{\odot}$  which, from what

we currently know, should have the same or similar spectral type (see e.g. Bonanos et al. 2004 and note that their values are present-day masses, not initial ones).

One way to decide which of the two options is correct is to search for radial velocity variations and possible eclipses, which is what Moffat et al. (2004) did. They found that A1 is an eclipsing binary with a 3.7724 day period. Olivier Schnurr and Tony Moffat (private communication) have recently measured the radial velocity variations of A1 and obtained masses of  $114 \pm 30 M_{\odot}$  and  $84 \pm 15 M_{\odot}$ , respectively. Interestingly, if we take those masses to be the initial ones, a  $114 M_{\odot} + 84 M_{\odot}$  unresolved object should have an apparent mass of  $157 M_{\odot}$ ; assuming some stellar mass loss during their lifetimes may add up to a few tens of solar masses to that value. The observed evolutionary masses lie between  $159 M_{\odot}$  and  $217 M_{\odot}$ , which is in very good agreement with the Schnurr and Moffat result.

Schnurr and Moffat (in preparation) have also found that C is a binary with an 8.92 day period, so at least two of the WN objects in NGC 3603 are not single. B shows no signs of radial velocity variations so far but that does not mean that it is not a binary, since most massive binaries have separations (and some, also inclinations) that make their motions hard to detect. On the other hand, both A1 and C are overluminous in X-rays (Moffat et al. 2002), usually a sign of binarity since intense X-ray emission is produced in wind-wind interactions but B is normal. Then again, that does not preclude B from being a binary with a separation large enough not to emit extra X-rays but still small enough not to have its two components resolved by ACS/HRC.

In summary, our analysis of NGC 3603 has found out that the existence of 2-3 objects with apparent masses above  $120 M_{\odot}$  would be expected as the result of the observed number of stars in the cluster and its IMF below that limit without having to invoke the existence of stars with real masses above  $120 M_{\odot}$ . The underlying hypothesis is that most or all massive stars in NGC 3603 are members of binary systems. Independent data have shown that indeed two of those stars are binaries and the currently available results for the third one leave room for the decision to go either way. The measurement of  $\gamma$  could be revised slightly when the additional ACS data are processed. When we do that in a future paper, we will apply CHORIZOS to calculate individual extinction corrections for each star, derive a distance from the data, and do a comparison between the resulting color-magnitude diagram with the one in Fig. 1.

### 3.2. R136

From a historical point of view, R136 (HD 38268), the core of 30 Doradus, is an excellent case study on the problems caused by multiplicity, either real or induced by chance superpositions. Walborn (1973), noting the WR features in its spectrum, compared it to NGC 3603 and suggested that it could be a Trapezium-like system made out of Wolf-Rayet and other early-type O stars. On the other hand, Cassinelli et al. (1981) dismissed that the central object, R136a, could be made out of “30 O3 or WN3 within a space of 0.5 arcsec (0.1 pc)” and proposed instead that it was a single supermassive star with  $2500 M_{\odot}$ . A few years later that alternative was shown to be false first by Moffat & Seggewiss (1983) by detecting spectral variations within R136 and later by Weigelt & Baier (1985) by using speckle interferometry to resolve R136a into eight individual sources, something which was later confirmed with HST (Weigelt et al. 1991).

Several later HST studies have analyzed the stellar composition of R136, of which the most complete is that of Massey & Hunter (1998). They obtained FOS spectroscopy of all the bright point sources in the core and combined it with PC (WFPC2) photometry to derive a color-magnitude diagram of the massive stars. In a follow-up paper, Massey et al. (2002) observed four spectroscopic eclipsing binaries and measured their masses. They also detected another five eclipsing binaries, indicating that massive binaries are also common in R136. From their data, Massey & Hunter (1998) measured a Salpeter- or Kroupa-like IMF with  $\gamma$  between  $-2.3$  and  $-2.4$  for the range  $15\text{--}120 M_{\odot}$ . That value, however, does not correspond to R136 alone but also includes the inner part of the 30 Doradus halo. In any case, for lack of better information, it will be the value assumed here.

R136 is roughly seven times farther away than NGC 3603. Also, 30 Doradus has never been observed with ACS (either WFC or HRC) and the best data currently available were obtained with the PC on WFPC2 (that was what Massey & Hunter 1998 used), which has a factor of 1.6 lower pixel size than HRC. Therefore, if R136 and NGC 3603 had similar stellar densities at their centers, one would expect crowding to be  $(1.6 \times 7)^2 \approx 125$  times worse in the former. The difference in resolution is readily apparent when one compares Figs. 14 and 16.

Let us quantify how important crowding is within a  $1''$ -radius circle centered on R136. Doing aperture photometry on the F555W data, obtaining  $A_V$  from the data in Massey & Hunter (1998), and using CHORIZOS to estimate the conversion to the  $V$  passband, I derive an extinction-corrected  $m_V$  of 9.29. Assuming an effective pixel radius of 2.5 real pixels I ob-

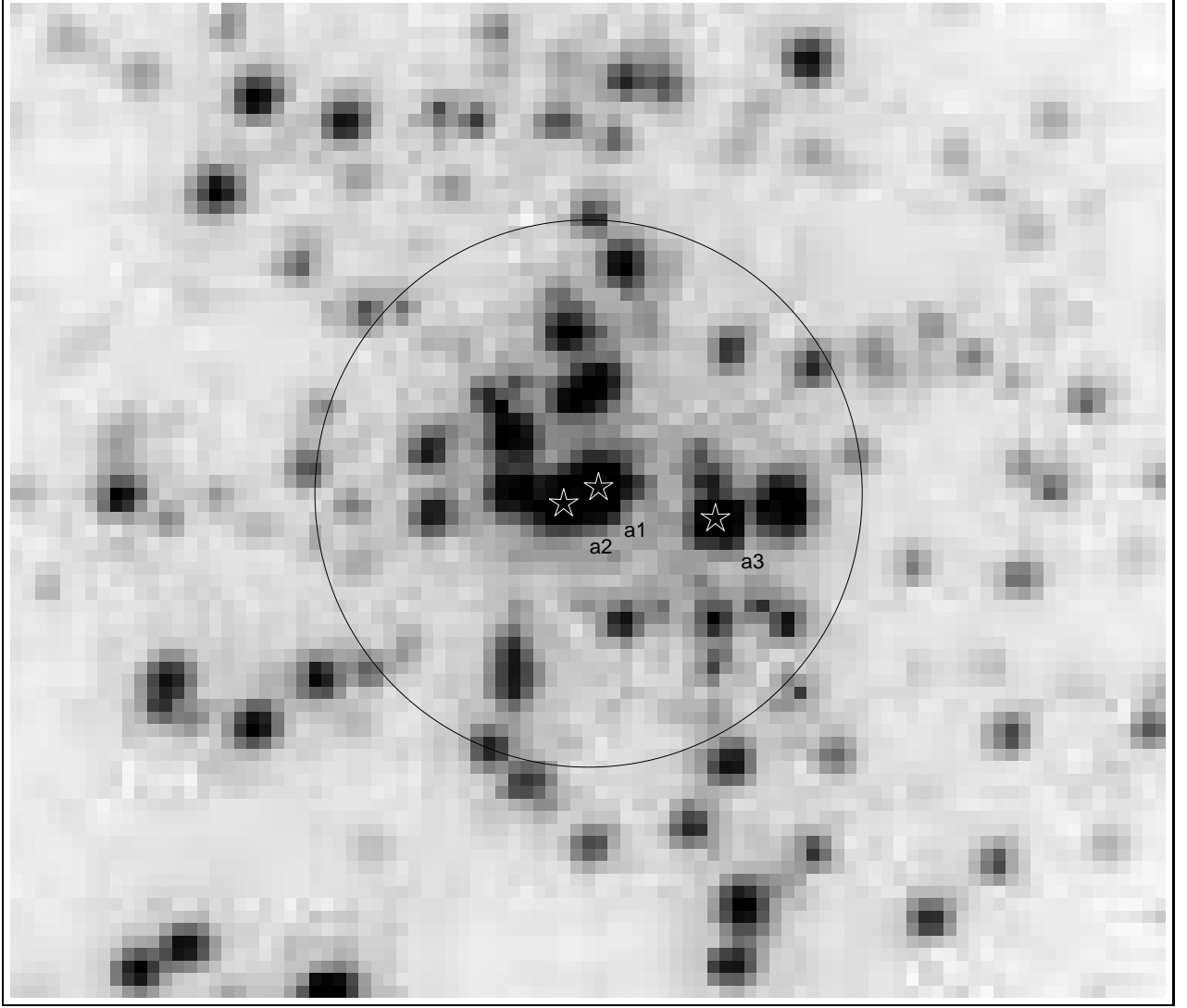


Fig. 16.— PC (WFPC2) F555W image of R136. The three WNha objects are marked and a circle with radius of  $1''$  centered on the cluster has been drawn. A square-root scale between 0 and 400 counts has been used in order to show both the bright and the dim stars. The pixel size is  $0''.0455$ , the field size is  $4''.23 \times 3''.64$  ( $93 \text{ px} \times 80 \text{ px}$ ), and the vertical direction is  $37.8^\circ$  West of North. The physical size ( $1.0 \text{ pc} \times 0.9 \text{ pc}$ ) is similar to that of Fig. 14.

tain  $m_{V,\text{epx}} = 14.01$ . For assumed values of 1 million years (age)<sup>17</sup>, LMC (metallicity), and Kroupa (IMF), the value  $M_{V,1} = 0.79$  is obtained. Finally, assuming a distance of 50 kpc, Eqn. 1 yields  $N_{\text{epx}} = 129$ . The value is relatively robust to small variations in the assumed parameters. Therefore, the  $n = 7$  results of the second experiment (if binaries are not abundant in R136) and the  $n = 6$  results of the third experiment (if binaries dominate) should be the reference for the analysis of the PC data of R136. This means that all the objects within the circle in Fig 16 have to be the superposition of a large number of stars (the majority of them being of low mass).

Using  $f_{a,64b}$  we obtain that 1.6% of the 77 effective pixels within  $1''$  are expected to contain one object above  $120 M_{\odot}$ . The equivalent value for  $f_{a,128s}$  is 0.6%. This translates into 1.3 and 0.5 stars, respectively<sup>18</sup>. How does this compare with the observations? Using the currently preferred low-temperature-scale values of Massey & Hunter (1998), the three most massive stars in the region are R136a1, a2, and a3, with masses of  $136 M_{\odot}$ ,  $122 M_{\odot}$ , and  $120 M_{\odot}$ , respectively. Those observed masses agree very well with the values predicted by the experiments in this paper, especially if binaries dominate. It is also interesting to point out that three of the four most massive objects with spectral types in the larger region explored by Massey & Hunter (1998) are within the  $1''$  radius considered here. One explanation would be that the most massive stars form preferentially in very dense environments. However, there are five other stars with similar spectral types (WNha and O3 If\*/WN) outside the most crowded regions with masses only slightly lower (between  $103 M_{\odot}$  and  $120 M_{\odot}$ ). Hence, a reasonable alternative is that all of those stars have similar masses and that the extra measured mass in R136a1, a2, and a3 is simply due to the increased likelihood of chance superpositions there.

R136 was the cluster used by Weidner & Kroupa (2004) and Koen (2006) and one of the clusters in the sample used by Oey & Clarke (2005) to derive an  $m_{\text{max}}$  around  $150 M_{\odot}$  (with varying degree of uncertainty around the value). All of those works used the Massey & Hunter (1998) values for the masses which, even for the low-temperature scale, include at least a star with a mass of  $136 M_{\odot}$  (R136a1). Of course, the existence of a single star with such a mass invalidates the possibility that  $m_{\text{max}}$  is lower than that value. However,

---

<sup>17</sup>R136 could hardly be significantly younger than that because it has already cleared of dense gas a large region around it. Also, if its age were older than 2 million years, its most massive stars would no longer be of WNha type.

<sup>18</sup>Note that the expected number of ultramassive stars is lower for R136 than for NGC 3603, despite the facts that the regions considered here have the same extinction-corrected absolute magnitude and that R136 is more crowded. The explanation resides in the different IMFs used for the calculation, Kroupa for R136 and top-heavy for NGC 3603.



if, as we have seen, the certain existence of chance superpositions and the likelihood that R136a1 is a binary<sup>19</sup> (as most massive stars are) are considered, then the real mass of the heaviest component in R136a1 could be  $120 M_{\odot}$  or even less.

What about deriving the true IMF slope from the observed AMF at the center of R136? Figs. 8 and 13 indicate that  $\Delta\gamma$  is in the range between 0.8 and 1.5 for 8-120  $M_{\odot}$  in the region within  $1''$ . That correction is too large and too dependent on the assumptions to be applied with confidence, so with the current data it is not possible to know the real IMF slope at the very center of R136. However, note that if a factor of 2 in (linear) effective pixel size is achieved, a dramatic change takes place. The relevant functions then are  $f_{a,32s}$  and  $f_{b,16s}$  and  $\Delta\gamma$  becomes  $\approx 0.10$ , which is a believable correction. Note also that in such a case, with  $\approx 300$  effective pixels and with a S/N large enough to have 100-150 of them populated with detected stars, the number of observed objects will be enough to derive a bias-free meaningful IMF ( $\sigma_{\gamma} \leq 0.2$ ) if the techniques in Paper I are used (see section 5 in Maíz Apellániz & Úbeda 2005).

Our summary for R136 is similar to that for NGC 3603. Even though there are stars with apparent masses above  $120 M_{\odot}$ , their detection can be explained by unresolved stars with real masses below that value. The main differences are that here the measured values are only slightly above the limit and that here the unresolved stars are a combination of chance superpositions and (likely) real multiple systems.  $\gamma$  cannot be reliably measured with the current data for the innermost regions of R136 but a moderate improvement in the quality (within the capabilities of HRC/ACS) should be sufficient to do the job.

## 4. Discussion

I have presented in this paper a simple method to quantify the effect of unresolved multiple systems and chance alignments on the heavy part of the mass functions of young stellar clusters and applied it to NGC 3603 and R136. Unresolved multiple systems introduce an intrinsic spread in the observed color-magnitude diagrams and can produce a population of AUMSs in a rich cluster. On the other hand, their effect on the apparent massive star MF slope is relatively small. Chance alignments can also produce AUMSs but only for large  $N_{\text{sup}}$ . As opposed to unresolved multiple systems, their effect on the AMF slope can be large.

To my knowledge, no similar method had been previously developed for those same circumstances. For the effect of binaries in the IMF of low-mass stars in the field and in

---

<sup>19</sup>Note that R136a1+a2 is not likely to be a bound system, as they are separated by at least 15 000 AU.

globular clusters, see Kroupa et al. (1991) and Sollima et al. (2007), respectively. For a similar (but more restricted) analysis to the one in this paper applied to intermediate-age clusters, see Sagar & Richtler (1991). Previous analyses for young clusters sometimes include a simplified correction with equal-mass binaries (e.g. Stolte et al. 2006) but in most cases binaries are included in the incompleteness analysis. An incompleteness test adds a large number of fake stars to the observed field and runs the output through the star detection algorithm to see how many of the fake objects are recovered. The percentage of unrecovered objects is then used to calculate an incompleteness correction. Such an analysis in reality is measuring two different effects: the weakest objects (those close to the detection limit) may be missed, even in an uncrowded region, either because Poisson/background fluctuations or read noise place them below the detection limit or because the details of the detection algorithm make it stop before reaching it. Alternatively, some brighter objects are missed because they are located close to an even brighter star that hides them under its PSF. The first effect (low S/N objects) should be quantifiable by studying the detector properties and the expected S/N as a function of magnitude. The second effect is more complex because it depends on the PSF (which may be or may be not well characterized) and, more importantly, the stellar distribution. For that reason, incompleteness tests need to be run on a specific dataset. Furthermore, a classical incompleteness test does not address the issue that the added fake stars may significantly modify the measured magnitude of the detected, brighter star, and, thus, alter the results of the mass function. The technique presented here does not attempt to substitute the correction of the first effect (low S/N objects) provided by incompleteness tests but only the second. It does so by [a] correcting the measured slope after it is fitted to the observed mass function rather than modifying the observed mass function before fitting it and [b] including the effect of the different mass detected when two stars are superimposed and not only counting the fraction of undetected objects. It also has the advantage of being easily quantifiable and applicable to the planning of future observations.

Having analyzed in detail NGC 3603 and R136, it is interesting to point out that no end-products of runaway collisions are seen there despite those two clusters being mentioned as likely candidates for them by Portegies Zwart et al. (2004). There are several possible explanations: [a] Runaway collisions do take place but the remaining products evolve so fast that those in NGC 3603 and R136 have already become black holes (this would require lifetimes of  $\approx 1$  million years). [b] Core collapse happens at a later stage, so the required time and density conditions are not satisfied in these clusters and ultramassive objects form only as a result of the merger of evolved objects. [c] Core collapse never happens and ultramassive objects never form. [d] The output of a massive stellar merger that would lead to an ultramassive stars is so unstable that it loses its excess mass almost immediately. Regarding

the latter possibility, it is notorious that very massive stars are very difficult to model and that our current knowledge of them is limited. Nevertheless, we know that there could be different mechanisms at work that would impede the formation of an ultramassive star via a merger: the resulting object may be directly above Eddington’s limit (Glebbeek & Pols 2007), so close to it that strange-mode instabilities overwhelm it (Townsend 2007), or may always rotate so fast that it surpasses the  $\Omega\Gamma$  limit (Maeder & Meynet 2000).

This article provides further evidence for the existence of a stellar upper mass limit at solar or near-solar metallicities. Furthermore, the analyzed data indicate that  $m_{\text{max}}$  may be as low as  $120 M_{\odot}$ . The situation for Population III stars is expected to be different, likely because the reduced opacity should place Eddington’s limit at higher luminosities and, hence, masses (see e.g. Zinnecker & Yorke 2007 and references therein).

Support for this work was provided by the Spanish Government Ministerio de Educación y Ciencia through grant AYA2004-08260-C03, grant AYA2007-64712, and the Ramón y Cajal Fellowship program and co-financed with FEDER funds. I would like to thank Tony Moffat and Phil Massey for providing me access to their work before publication; Nolan Walborn, Tony Moffat, and an anonymous referee for useful comments to previous versions of the manuscript; and Enrique Pérez and Miguel Cerviño for fruitful conversations on this topic.

## REFERENCES

- Anderson, J., & King, I. R. 2004, ACS Instrument Science Report 2004-15 (STScI: Baltimore)
- Bally, J., & Zinnecker, H. 2005, *AJ*, 129, 2281
- Belkus, H., Van Bever, J., & Vanbeveren, D. 2007, *ApJ*, 659, 1576
- Bonanos, A. Z., Stanek, K. Z., Udalski, A., Wyrzykowski, L., Żebruń, K., Kubiak, M., Szymański, M. K., Szewczyk, O., Pietrzyński, G., & Soszyński, I. 2004, *ApJL*, 611, L33
- Boyajian, T. S., Gies, D. R., Dunn, J. P., Farrington, C. D., Grundstrom, E. D., Huang, W., McSwain, M. V., Williams, S. J., Wingert, D. W., Fullerton, A. W., & Bolton, C. T. 2007, *ApJ*, 664, 1121
- Cassinelli, J. P., Mathis, J. S., & Savage, B. D. 1981, *Science*, 212, 1497
- Castelli, F., & Kurucz, R. L. 2003, in *IAU Symposium*, Vol. 210, *Modelling of Stellar Atmospheres*, ed. N. Piskunov, W. W. Weiss, & D. F. Gray, 20

- Cerviño, M., & Luridiana, V. 2006, *A&A*, 451, 475
- Crowther, P. A. 2007, *ARA&A*, 45, 177
- de Pree, C. G., Nysewander, M. C., & Goss, W. M. 1999, *AJ*, 117, 2902
- Drissen, L., Moffat, A. F. J., Walborn, N. R., & Shara, M. M. 1995, *AJ*, 110, 2235
- Eisenhauer, F., Quirrenbach, A., Zinnecker, H., & Genzel, R. 1998, *ApJ*, 498, 278
- Evans, C. J., Lennon, D. J., Smartt, S. J., & Trundle, C. 2006, *A&A*, 456, 623
- Figer, D. F. 2005, *Nature*, 434, 192
- Gamen, R., et al. 2007, in *Massive Stars: Fundamental Parameters and Circumstellar Interactions*, P. Benaglia and G. Bosch (eds.), to appear in *Rev. Mex. Astron. Astrofís.* (conference series)
- García, B., & Mermilliod, J. C. 2001, *A&A*, 368, 122
- Glebbeek, E., & Pols, O. R. 2007, *ArXiv e-prints*, 0710.1730
- Kobulnicky, H. A., & Fryer, C. L. 2007, *ApJ*, 670, 747
- Koen, C. 2006, *MNRAS*, 365, 590
- Kouwenhoven, M. B. N., Brown, A. G. A., Zinnecker, H., Kaper, L., & Portegies Zwart, S. F. 2005, *A&A*, 430, 137
- Krist, J. 1995, in *ASP Conf. Series, Vol. 77, Astronomical Data Analysis Software and Systems IV*, ed. R. A. Shaw, H. E. Payne, & J. J. E. Hayes, 349
- Kroupa, P., Gilmore, G., & Tout, C. A. 1991, *MNRAS*, 251, 293
- Kroupa, P., Tout, C. A., & Gilmore, G. 1993, *MNRAS*, 262, 545
- Lanz, T., & Hubeny, I. 2003, *ApJS*, 146, 417
- . 2007, *ApJS*, 169, 83
- Lejeune, T., Cuisinier, F., & Buser, R. 1998, *A&AS*, 130, 65
- Lejeune, T., & Schaerer, D. 2001, *A&A*, 366, 538
- Maeder, A., & Meynet, G. 2000, *A&A*, 361, 159

- Maíz Apellániz, J. 2004, *PASP*, 116, 859
- . 2006, *AJ*, 131, 1184
- Maíz Apellániz, J. 2007, in *ASP Conf. Series*, Vol. 364, *The Future of Photometric, Spectrophotometric and Polarimetric Standardization*, ed. C. Sterken, 227
- Maíz Apellániz, J., & Sota, A. 2008, in *Massive Stars: Fundamental Parameters and Circumstellar Interactions*, P. Benaglia and G. Bosch (eds.), to appear in *Rev. Mex. Astron. Astrofís.* (conference series), astro-ph/0702516
- Maíz Apellániz, J., & Úbeda, L. 2005, *ApJ*, 629, 873 (Paper I)
- Maíz Apellániz, J., Úbeda, L., Walborn, N. R., & Nelan, E. P. 2008a, in *Resolved Stellar Populations*, D. Valls-Gabaud and M. Chávez (eds.), astro-ph/0506283
- Maíz Apellániz, J., Walborn, N. R., Morrell, N. I., Niemela, V. S., & Nelan, E. P. 2007, *ApJ*, 660, 1480
- Maíz Apellániz, J., Walborn, N. R., Morrell, N. I., Niemela, V. S., & Nelan, E. P. 2008b, in *Massive Stars: Fundamental Parameters and Circumstellar Interactions*, P. Benaglia and G. Bosch (eds.), to appear in *Rev. Mex. Astron. Astrofís.* (conference series), astro-ph/0702514
- Mason, B. D., Gies, D. R., Hartkopf, W. I., Bagnuolo, W. G., Brummelaar, T. T., & McAlister, H. A. 1998, *AJ*, 115, 821
- Massey, P., & Hunter, D. A. 1998, *ApJ*, 493, 180
- Massey, P., Penny, L. R., & Vukovich, J. 2002, *ApJ*, 565, 982
- Melena, N. W., Massey, P., Morrell, N. I., & Zangari, A. M. 2007, *ArXiv e-prints*, 0712.2621
- Melnick, J., Tapia, M., & Terlevich, R. 1989, *A&A*, 213, 89
- Moffat, A. F. J. 1983, *A&A*, 124, 273
- Moffat, A. F. J., Corcoran, M. F., Stevens, I. R., Skalkowski, G., Marchenko, S. V., Mücke, A., Ptak, A., Koribalski, B. S., Brenneman, L., Mushotzky, R., Pittard, J. M., Pollock, A. M. T., & Brandner, W. 2002, *ApJ*, 573, 191
- Moffat, A. F. J., Drissen, L., & Shara, M. M. 1994, *ApJ*, 436, 183
- Moffat, A. F. J., Poitras, V., Marchenko, S. V., Shara, M. M., Zurek, D. R., Bergeron, E., & Antokhina, E. A. 2004, *AJ*, 128, 2854

- Moffat, A. F. J., & Seggewiss, W. 1983, *A&A*, 125, 83
- Nelan, E. P., Walborn, N. R., Wallace, D. J., Moffat, A. F. J., Makidon, R. B., Gies, D. R., & Panagia, N. 2004, *AJ*, 128, 323
- North, J. R., Tuthill, P. G., Tango, W. J., & Davis, J. 2007, *MNRAS*, 377, 415
- Nürnberg, D. E. A., Bronfman, L., Yorke, H. W., & Zinnecker, H. 2002, *A&A*, 394, 253
- Oey, M. S., & Clarke, C. J. 2005, *ApJL*, 620, L43
- Öpik, E. J. 1924, *Tartu Obs. Publ.*, 25
- Portegies Zwart, S. F., Baumgardt, H., Hut, P., Makino, J., & McMillan, S. L. W. 2004, *Nature*, 428, 724
- Portegies Zwart, S. F., Makino, J., McMillan, S. L. W., & Hut, P. 1999, *A&A*, 348, 117
- Rauw, G., De Becker, M., Nazé, Y., Crowther, P. A., Gosset, E., Sana, H., van der Hucht, K. A., Vreux, J.-M., & Williams, P. M. 2004, *A&A*, 420, L9
- Reipurth, B., Guimarães, M. M., Connelley, M. S., & Bally, J. 2007, *AJ*, 134, 2272
- Sagar, R., & Richtler, T. 1991, *A&A*, 250, 324
- Sollima, A., Beccari, G., Ferraro, F. R., Fusi Pecci, F., & Sarajedini, A. 2007, *MNRAS*, 380, 781
- Stolte, A., Brandner, W., Brandl, B., & Zinnecker, H. 2006, *AJ*, 132, 253
- Stolte, A., Brandner, W., Brandl, B., Zinnecker, H., & Grebel, E. K. 2004, *AJ*, 128, 765
- Sung, H., & Bessell, M. S. 2004, *AJ*, 127, 1014
- Townsend, R. 2007, *ArXiv e-prints*, 0709.0761
- Walborn, N. R. 1973, *ApJL*, 182, 21
- Weidner, C., & Kroupa, P. 2004, *MNRAS*, 348, 187
- Weigelt, G., Albrecht, R., Barbieri, C., Blades, J. C., Boksenberg, A., Crane, P., Deharveng, J. M., Disney, M. J., Jakobsen, P., Kamperman, T. M., King, I. R., Macchetto, F., Mackay, C. D., Paresce, F., Baxter, D., Greenfield, P., Jedrzejewski, R., Nota, A., & Sparks, W. B. 1991, *ApJ*, 378, L21

Weigelt, G., & Baier, G. 1985, A&A, 150, L18

Yungelson, L. R., van den Heuvel, E. P. J., Vink, J. S., Portegies Zwart, S. F., & de Koter, A. 2008, A&A, 477, 223

Zinnecker, H., & Yorke, H. W. 2007, ARA&A, 45, 481